Prediction of Formation of Amorphous Alloys during Annealing of Ti-binary Alloys and Validation of the same

Contract

Asian Office Aerospace Research and Development

Department of the Air Force

National Metallurgical Laboratory, Jamshedpur

831 007, India

Report Documentation Page

Form Approved
OMB No. 0704-0188

1. REPORT DATE	2. REPORT TYPE	3. DATES COVERED
22 NOV 2009	**FInal**	**11-01-2008 to 11-05-2009**

4. TITLE AND SUBTITLE
Prediction of Formation of Amorphous Phases During Annealing of Titanium Binary Alloys and Validation of the Same

5a. CONTRACT NUMBER
FA48690810005

5b. GRANT NUMBER

5c. PROGRAM ELEMENT NUMBER

6. AUTHOR(S)
S Ranganathan

5d. PROJECT NUMBER

5e. TASK NUMBER

5f. WORK UNIT NUMBER

7. PERFORMING ORGANIZATION NAME(S) AND ADDRESS(ES)
National Metallurgical Laboratory,Burma Mines, Jamshedpur, Jharkhand State,Jamshedpur 831-007,India,IN,831-007

8. PERFORMING ORGANIZATION REPORT NUMBER
N/A

9. SPONSORING/MONITORING AGENCY NAME(S) AND ADDRESS(ES)
AOARD, UNIT 45002, APO, AP, 96337-5002

10. SPONSOR/MONITOR'S ACRONYM(S)
AOARD

11. SPONSOR/MONITOR'S REPORT NUMBER(S)
AOARD-074038

12. DISTRIBUTION/AVAILABILITY STATEMENT
Approved for public release; distribution unlimited

13. SUPPLEMENTARY NOTES

14. ABSTRACT

Observation of an amorphous phase produced on annealing has excited scientists since the process can be easily controlled leading to bulk amorphous alloys that can find several technological applications. However, this phenomenon has to be explored further and understood in order to exploit it. It is important to understand the thermodynamics of this unusual phase transformation. This can lead to a better understanding of the fundamental aspects of this process. This can further open up new avenues of research also. Hence, the present investigation was carried out to model the thermodynamics of the phenomenon of this inverse melting in Ti-binary alloys and validate the same.

15. SUBJECT TERMS
Thermodynamics, Titanium Alloy

16. SECURITY CLASSIFICATION OF:			17. LIMITATION OF ABSTRACT	18. NUMBER OF PAGES	19a. NAME OF RESPONSIBLE PERSON
a. REPORT	b. ABSTRACT	c. THIS PAGE			
unclassified	**unclassified**	**unclassified**	**Same as Report (SAR)**	**77**	

Prediction of Formation of Amorphous Alloys During Annealing of Ti-binary Alloys and Validation of the Same

CONTENTS

Prediction of Formation of Amorphous Alloys During Annealing of Ti-binary Alloys and Validation of the Same

1. Introduction

Inverse melting is a phenomenon where a crystalline phase becomes amorphous on cooling. This is counter-intuitive since a crystalline phase becomes disordered usually on heating when it becomes a liquid. This inverse phenomenon has been observed in several binary metallic systems, most of them based on titanium. For example, in the Ti-Cr system, an alloy rich in titanium has a b.c.c (body centered cubic) structure at high temperature. An alloy held at this temperature, say $1100^{o}C$, retains this structure on cooling to room temperature. When the alloy is heated to $600^{o}C$, the b.c.c structure transforms to an amorphous phase. The overall temperature cycle of this process corresponds to cooling the b.c.c. structure from 1100°C to 600°C during which it transforms to an amorphous phase (fig. 1.1). A similar phenomenon is obtained in other binary alloy systems such as Ti-Mn,Ti-Cu,Ti-Nb etc.

It is also important to note that a phase which is crystalline at room temperature (i.e the bcc phase) transforms to the amorphous phase on heating. This is, again, unusual. Heating a system should transform it into an equilibrium state rather than producing a meta-stable structure. Observation of an amorphous phase produced on annealing has excited scientists since the process can be easily controlled leading to bulk amorphous alloys that can find several technological applications. However, this phenomenon has to be explored further and understood in order to exploit it. It is important to understand the thermodynamics of

this unusual phase transformation. This can lead to a better understanding of the fundamental aspects of this process. This can further open up new avenues of research also. Hence, the present investigation was carried out to model the thermodynamics of the phenomenon of this inverse melting in Ti-binary alloys and validate the same.

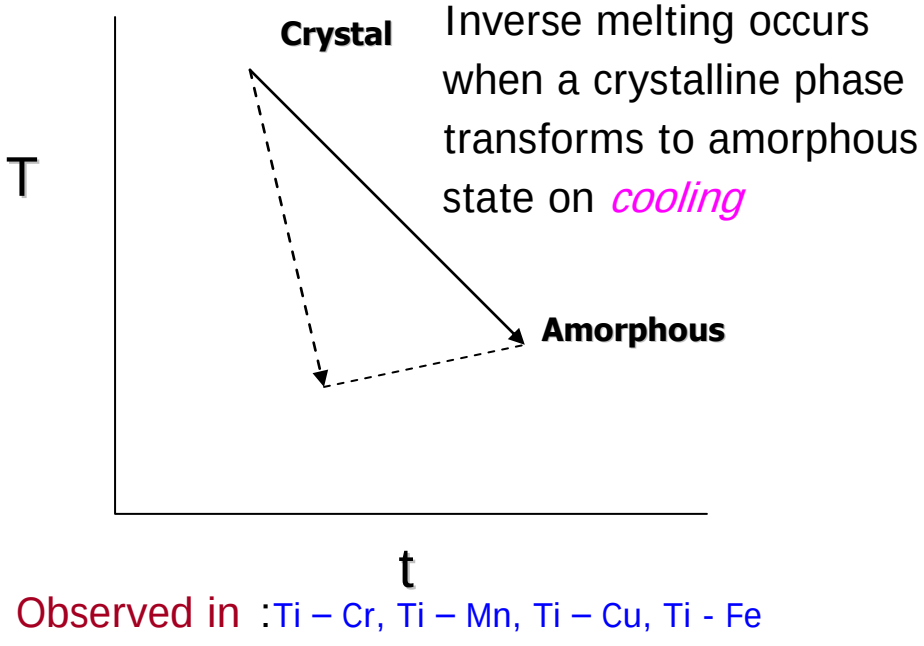

Fig. 1.1 Inverse Melting in Alloys

2. Aim and objectives

Aim

To predict, from the principles of thermodynamics of non-equilibrium phase transformation, the temperature and composition range in which amorphous alloys can be formed during annealing of titanium binary alloys and validation of prediction through experimental investigation.

Objectives

(1) To construct phase transformation diagram for titanium binary alloys such as Ti- Cr,Ti-Cu,Ti-Mn,Ti-Nb.

(2) To predict the composition and temperature range of formation of amorphous alloys in the binary system.

(3) Preduction of amorphous alloys through annealing and validation of the predictive model.

(4) Investigation on the production of amorphous alloys in these systems through the annealing route.

(5) Modeling the influence of ternary addition on the formation of amorphous phase in titanium based alloy system through the construction of ternary Transformation Diagram.

3. Inverse Melting in Ti-based Alloys

Considerable amount of research has been carried out on the phenomenon of Inverse Melting in titanium-based alloys. Most of this has been on the Ti-Cr system. There have been reports on the observation of this phenomenon is other alloy system also. Blater and von Allman(1) produced metastable crystalline and amorphous phases using the technique of pulsed laser-quenching. These meta-stable phases were produced in Au-Ti and Cr-Ti films. When the quenched samples were subjected to annealing, the meta-stable crystalline phases modified into amorphous phases for some of the alloy compositions in both the systems. In the case of the Cr-Ti alloy, the amorphous phase reverted to the crystalline state on further annealing at higher temperatures. Electron gun deposition was used for producing metallic films 150 nm thick. The films were subjected to laser quenching and to annealing in vacuum furnaces (10^{-6} mbar or better). X-ray diffractometry and electrical resistivity measurements were used for characterizing the alloys. The absence of lines and the presence of a halo in the XRD along with an increase in electrical resistance led to the inference of the presence of an amorphous phase.

In the case of the Au-Ti system, the intermediate composition produced meta-stable crystalline phases such as (Au_4Ti+Au_3Ti) instead of equilibrium phases, viz.(Au_2Ti +AuTi) on leaser quenching. The $Au_{60}Ti_{40}$ phase became amorphous on annealing at 350°C. Cr-Ti alloys with X_{Ti}>0.6 (X_{Ti} – atom fraction of titanium), the as-quenched films retained the bcc structure. These films turned amorphous on annealing at 600°C for 30 minutes. When these amorphous films were further annealed at 800°C,

they formed either the equilibrium phases or the reverted to the bcc structure, depending on the composition and the substrate used. Films on W-substrate cycled between the amorphous and 'β' (bcc) phase on annealing at 600°C and 800°C, respectively. The β-phase had the same composition as the amorphous phase. This is highlighted by the authors as a case of diffusion-less amorphitization. The authors have constructed Free Energy-Composition Diagrams at 600°C and 800°C which show that the amorphous phase has a lower free energy compared to the β phase 600°C between compositions X_{Ti}=0.3 and X_{Ti}=0.7. At 800°C, the amorphous phase is less stable compared to the β phase at X_{Ti}= 0.7. The authors surmise that this causes the reversible

$$\beta \rightarrow \text{amorphous} \qquad (3.1)$$

transformation at this composition.

The thermodynamic and kinetic criteria required for the formation of amorphous phase through the annealing of the crystalline phase has been examined(2). These authors note that a number of alloy systems form amorphous phase when heterogeneous mixtures of constituent elements are subjected to annealing, cold working, milling etc. Certain alloys such as the Cr-Ti alloys vitrify spontaneously on annealing at low temperatures. This process is termed as "spontaneous vitrification". The amorphous phase is interspersed with a Ti-rich *bcc* phase. The process here involves retaining a high temperature crystalline phase at room temperature, through relatively slow cooling and then annealing the meta-stable crystalline phase at low temperatures. Since "spontaneous vitrification" odes not require rapid quenching, it might be possible to scale it up. This phenomenon has been observed in $Cr_{40}Ti_{60}$ alloy several millimeters in size. The authors define "spontaneous vitrification" (SV) as a process in

which a meta-stable crystalline phase transforms to an amorphous phase of the same composition upon low temperature annealing.

SV occurs if the following criteria are satisfied: (a) there is a large driving force for the formation of the amorphous alloys and (b) competing transformation such as equilibrium crystal growth is prevented during the preparation and annealing of the meta-stable crystalline phase "m". When this meta-stable phase tends to decompose to form the equilibrium phases, SV occurs. The annealing temperature must be less than the first crystallization temperature T_x, of the glass formed. T_x is of the order of the glass transition temperature. Hence, SV is an inherently slow process. The amorphous phase must have a free energy less than that of the meta-stable phase "m". The authors introduced an enthalpy difference of 8 kJ/mol between the extrapolated melt and the glass in order to ensure that this criterion was obeyed. It was hypothesised that short-range order could make the glassy phase more stable compared to the undercooled melt. A softening of the lattice on glass formation contributes an additional factor for the formation of the amorphous phase. This decrease in the lattice strain was assumed by the authors to be the driving force for SV. Therefore, "phases with a large lattice strain energy are susceptible to SV in general"(2). For the β-$Cr_{40}Ti_{60}$ alloy, the strain energy is about 7 kJ/mol. Combined with the free energy difference of 8 kJ/mol between the glass and the under-cooled melt, the driving force for SV is about 1.8 kJ/mol. The driving force for equilibrium transformation $\beta \rightarrow \alpha$-Ti + Cr_2Ti is about 3.5 kJ/mol but this reaction is inhibited kinetically.

Therefore, for SV to occur : (a) a high temperature phase that can be easily retained at room temperature on rapid cooling must be present; (b)

at temperatures less than the stability range of the metastable phase 'm', an extended two-phase field must be present, spanning about 10 at% on either side; the equilibrium phases must have, preferably, crystal structures different from that of 'm'; (c) the metastable phase must have a large strain energy, about 5 kJ/mol. A number of systems satisfying these criteria have been identified. Thin films, about 150 nm thick, were prepared from these alloys on sapphire substrates. The metastable phases were prepared by laser quenching. These were annealed at low temperatures for about 60 minutes. XRD was used to confirm the presence of the amorphous phase.

The systems investigated could be classified into three broad groups: (a) systems that failed to form the meta-stable phase 'm' (such as Al-Zn, Au-Mn and Cr-W); (b) systems that formed the meta-stable phase 'm', but did not vitrify (such as Ag-Cu, Ag-Cr, Au-Fe,Au-Ni,Cr-Mo,Cr-Ni, Pd-Ti, Ti-V) and systems where vitrification was observed (such as Cr-Ti,Cu-Ti,Fe-Ti, Mn-Ti,Co-Nb, Ni-Nb). Marginal cases were Au-Ni and Ti-V. All the systems that exhibited SV had bcc-type 'm' phase. This might be because amorphous phases are easily nucleated from *bcc* lattice which has a similar coordination number.

Blatter and Gfeller(3) investigated spontaneous vitrification of the β phase produced in Cr-Ti alloys through different routes. TEM, XRD, electrical resistivity and hardness were used for characterizing the alloys. The method of preparation of the β (bcc) phase appeared to be a critical parameter in the successful vitrification of the alloy. This study showed that SV was observed only in thin films prepared by laser quenching and in bulk samples prepared by water quenching. Splat-cooled samples

showed no vitrification in spite of the fact that these samples also exhibited the presence of pure β-structure. The XRD of the splat-cooled samples showed sharp peaks and their relative intensities were in perfect agreement with the intensities calculated for a topologically perfect and chemically random Cr-Ti phase. In the case of the laser-quenched and water-quenched samples, the peaks were broader and were less intense, particularly at high indices. The topological coherence length was estimated to be about 10 nm for the bulk and the thin film samples and it was 35 nm in the case of the splat-cooled samples. TEM showed that the film and bulk samples showed a periodicity of 10 nm for the contrast modulation, matching with the coherence length estimated from XRD measurements. The SAD of these samples showed evidence for strong ω-like (tetragonal) distortions and the presence of anisotropically-strained lattice.

Thin film and bulk samples have strongly distorted and anisotropically strained β phase. These deficiencies provide a large number of incoherent sites as nucleation centers for the amorphous phase. In the case of bulk samples, coherent precipitates started appearing after 5 minutes of annealing at 600 °C. The alloy had a composition of X_{Ti}=0.6. The evolving precipitate had a bcc structure whose lattice constant was close to that of the parent β phase. However, the two phases differed in orientation. The precipitate was rich in titanium at metastable equilibrium with the amorphous phase. Formation of the amorphous phase coincided with the formation of the coherent precipitate. Samples were annealed in ultra-high vacuum for several hours to achieve spontaneous vitrification. SAD of the samples showed that the amorphous matrix was interspersed with

crystal grains which occupied about 10% of the volume and measured 3-5 nm. They consisted of β' and ω phases.

The spontaneously vitrified $Cr_{40}Ti_{60}$ alloy had a hardness that was about 40% higher than that of the parent alloy. The longitudinal sound velocity decreased by about 10%. This indicated an elastic softening. The mechanical properties were independent of the amount of crystalline inclusions. These properties were dominated by the amorphous matrix. However, the electrical properties were influenced by the crystalline inclusions.

This study demonstrated that phases with a disturbed *bcc* lattice, as obtained by laser quenching and water quenching, vitrified readily whereas perfect *bcc* phases, produced by splat cooling did not vitrify. This difference in behaviour is attributed to the presence of a large number of nucleation sites for the amorphous phase in the former case. High cooling rate generates these sites in laser quenching. In the case of the water-quenched samples, there is incipient decomposition which encourages the formation of the amorphous phase.

Blatter et.al.(4) investigated the role of defects in the SV of β-Cr-Ti alloy. From their experiments, they inferred a direct correlation between the structural evolution of the alloy and the defect concentrations. These authors noted that earlier experiments had established that ***crystalline*** $\rightarrow$ ***amorphous*** transformation did not take place in diffusion couples if some disordered nuclei were not present. In the case of SV, it has been observed that vitrification began preferentially at sites of inherently high defect concentration such as free surfaces and grain boundaries. In their investigations(4), the authors produced splat-cooled β-$Cr_{40}Ti_{60}$ alloys of

thickness 30-50 μm. They were subjected to irradiation by H^+ and He^{2+} ions. The irradiated samples were annealed in vacuum better than 10^{-6} atm. at temperatures ranging from 540 to 600°C. XRD and SEM were used for monitoring the structural evolution. DSC was used for measuring the specific heats. XRD peaks of the annealed samples indicated the presence of an amorphous phase. In some samples, the β-phase reflections were split pointing to a tendency for chemical partitioning due to a spinodal driving force. Under heavy irradiation, equilibrium phases, α-Ti and Cr_2Ti started appearing in the annealed samples.

When the sample is not irradiated, the β structure of the splat-cooled samples showed no transformation up to 600 °C. Equilibrium phases were formed at 600°C, in these samples. The irradiated samples showed transformation at 540°C. A transient amorphous phase appeared to form at early stages of annealing. This study showed that a minimum defect concentration was required for the formation of the amorphous phase.

DSC measurements on non-irradiated samples showed an enthalpy relaxation of 450 J/g.atom around 400 °C. The irradiated samples showed an additional exothermic peak around 225 °C and a step-like increase of specific heat at about 500 °C. The exothermic peaks appeared only during the first heating cycle. The step appeared reversibly during the heating and cooling cycles. However, the step disappeared after equilibrium phases were formed during prolonged annealing. The authors found an apparent relationship between the step height and the defect concentration. The authors argued that the occurrence of the reversible step in the specific heat reflected "the freezing and unfreezing of some degree of freedom". At temperatures below the step, the Dulong-Petit law

was operative and only the vibrational modes were active. Above this temperature, an additional diffusion mode was active. Molecular dynamics simulations have demonstrated (5,6) that defects could induce vitrification. The simulation showed that an amorphous phase was formed from the crystal if the concentration fo the defect was high enough. This was in excellent agreement with experimental studies (4).

The possibility of spontaneous vitrifictaion in the Ti-Cr system was investigated constructing thermodynamic models of various phases in the system (7). Miedma's model was used for describing the thermodynamic properties of the amorphous phase. This study showed that amorphisation was possible in this system at 77 K at X_{Ti}=0.6. However, the calculations showed that the β phase was more stable compared to the amorphous phase, except at low temperatures. The stability gap increases with increase in temperature due to a reduction in the elastic contribution to the heat of formation of the β phase. This explained why the splat-cooled samples did not show SV. On the other hand, SV occurred in distorted *bcc* lattice because this lattice had a higher enthalpy of formation, making it less stable compared to the amorphous phase. The authors concluded that it was a lucky accident that an alloy of composition X_{Ti}=0.7 transformed to the *bcc* phase at 1073 K since the free energy of the *bcc* phase was less than that of the amorphous phase at this temperature.

Kim and Lee(8) investigated the kinetics of the spontaneous transformation(SV) of $Cr_{40}Ti_{60}$ alloy. The authors note that the amorphous phase formed during SV in this alloy contains some crystalline inclusions whose nature remains unevaluated. In their studies, the authors(8) measured the activation energy for vitrification through XRD and that for

equilibrium transformation from DTA. Cubes of $Cr_{40}Ti_{60}$ alloy, 5 mm thick, were equilibrated at 1573 K, followed by quenching in water. Equilibration was carried out in N_2 atmosphere. XRD of the quenched sample confirmed the presence of the β phase. The quenched sample was annealed below 893 K for 5 hours in N_2 atmosphere. The annealed samples were slices cut from the quenched sample to 1 mm thickness. XRD and TEM were used for studying the vitrification process. Bragg peaks of the β phase were not observed in the annealed samples. Small diffraction peaks which were difficult to index were seen along with a super-imposed halo trace. The observations were similar to those of Blatter and Allmen() who suggested that these peaks were Ti-rich bcc solid solution and a meta-stable, transient ω peak. The latter authors have argued that the formation of crystalline inclusions could not be avoided. Diffraction pattern of the annealed samples under TEM showed a broad halo indicating the presence of an amorphous phase. However, this pattern also contained resolved, scattered spots confirming the existence of a new second crystal phase.

DTA of the β-$Cr_{40}Ti_{60}$ powder sample showed two exothermic peaks. One was broad, in the low temperature range and the other was sharp, in the high temperature range. The low temperature peak was probably related to stress relaxation. The high temperature peak corresponded to the decomposition of the β phase to the equilibrium phases Cr_2Ti and α-Ti. The presence of the β phase in the sample annealed at 1066 K was anomalous since it was not an equilibrium phase at this temperature. The lattice parameter of this β phase (a=3.207 A) was different from that of the as-quenched β phase (a=3.120 A).From published data on the lattice parameters of the β phases; the composition of the newly formed β phase

was calculated to be $Cr_{17}Ti_{83}$. From the Kissinger plot of the high temperature peak of DTA, the activation energy for equilibrium phase formation was estimated to be 62.0 kW/mol. This value could be related to the inter diffusion of Ti and Cr atoms in the matrix.

For studying isothermal transformation kinetics, electrical resistivity measurements are generally used. However, it is difficult to prepare samples without defects such as cracks caused by quenching due to the small size of the samples. Hence, XRD was the only viable technique for studying the kinetics of transformation. An internal standard method was used for this purpose(8). The relationship between the transformed fraction and the reaction time could be described by the Johnson-Mehl-Avarami equation:

$$F = 1-\exp[-(kt)n] \qquad (3.2)$$

Where, 'f' is the fraction transformed, 'k', is the rate constant; 'n', the rate constant exponent and 't', the reaction time. From this study of the kinetics of transformation, the activation energy for SV was estimated to be 46.2 kca/mol. This is less than that for equilibrium transformation. Because of this difference in activation energies, SV precedes the equilibrium transformation. Data available in literature showed that the activation energies for the diffusion of Cr in 18 at% and 10 at% Ti-Cr alloys were 44.5 kcal/mol and 40.2 kcal/mol, respectively. Hence, the authors (8) surmised that the activation energy for SV was closely related to the diffusion of Cr atoms in the Ti matrix. The titanium atoms are frozen in the matrix in reaction due to the large size of the titanium atom compared to that of the chromium atom.

Various techniques such as calorimetry, dilatometry, resistivity measurements and XRD were used by Wirz and Blatter(9) to study the transformation preceding amorphisation in the Ti-Cr system. These authors point out that studies have shown the spontaneous vitrification process consisted of a number of steps. DSC studies were carried out using sample weights of 40 mg. During the first heating cycle of the DSC of the as-quenched β $Cr_{40}Ti_{60}$ sample, an exothermic reaction occurred. This reaction was not reversible and did not appear during the subsequent cycles. The temperature and enthalpy of this reaction were represented by T_H and ΔH, respectively. The exothermic reaction was followed by a step-like increase of the specific heat-capacity. The specific heat reaction occurred reversibly during successive heating and cooling cycles. The specific heat reaction occurred at a temperature T_s. The dilatometer traces were similar to those of DSC. There was an irreversible change ΔV, at T_H and a reversible change$\Delta\alpha$, at T_s. The values of ΔH and ΔV depended on the concentration of the alloy and also on the preparation history. The step height was not influenced by the preparation method. The apparent co-efficient of electrical resistivity decreased abruptly and substantially at 435 °C, which corresponded to the temperature T_H. The alloy $Cr_{20}Ti_{80}$ exhibited neither the enthalpy reaction nor the drop in the apparent co-efficient of resistivity. The specific heat reaction had no counter part in the resistivity data.

Isothermal measurements were also made on the alloys at various temperatures. Dilatometry traces showed an initial contraction followed by a much larger contraction over a period of several hours (at 440 °C). The first contraction was associated with a decrease in resistivity whereas the second one was associated with an increase in resistivity. XRD data

showed correlation with the first contraction whereas the second one apparently left the lattice unchanged. When the isothermally pre-annealed samples were heated above T_s, a third process also became apparent. The material expanded by an amount similar to the second contraction but the resistivity decreased to its former value. The nature of the last two contractions has not been understood.

It may be possible to associate the enthalpy reaction with a vitrification process. The amorphous phase can be expected to show a glass transition in line with the specific heat reaction observation. However, XRD of the "glass' produced by the enthalpy reaction shows long-range order. Only after prolonged annealing above T_s, amorphisation occurs. It is inferred that the long-range order phase from the enthalpy reaction and the amorphous phase formed above T_s are the same thermodynamic phase, to a first approximation.

There is a large volume expansion and increase in electrical resistivity when the amorphous phase is formed. It is argued by the authors(9) that the increase in volume most likely places severe kinetic constraints on bulk amorphisation. The irreversible exothermic reaction and the specific heat reaction are essential for amorphisation. If either of the two effects is missing, amorphisation does not occur, as in the case of $Cr_{20}Ti_{80}$. The specific heat transition is also noticed only in the presence of "holes". Splat-cooled $Cr_{40}Ti_{60}$ samples do not show specific heat transition. They do not vitrify either. The authors conclude that long-range diffusion is generally not required for spontaneous vitrification since it is a polymorphous transition.The enthalpy reaction is thermally-activated. The activation energy for this reaction was estimated to be 2.0 ± 0.3 eV.

Drop calorimeter and DSC were used by Ohsake et.al.(10) to measured the enthalpy and specific heat of the liquid and β phases in the $Cr_{40}Ti_{60}$ alloy. The authors point out that thermodynamic criterion requires that the free energy of the amorphous phase must be less than that of the β phase for the latter to transform to the amorphous phase. The Gibbs Free Energy difference between the liquid and the β phase is given by

$$\Delta G(T) = (\Delta H_f + \int C_p\, dT) - T(\Delta S_f + \int(\Delta C_p/T)\, dT \qquad (3.3)$$

Here, ΔH_f and ΔS_f are the enthalpy and entropy of fusion, respectively; T_m is the melting point which is taken as the congruent melting temperature. $\Delta C_p = (C_p^l - C_p^\beta)$.

$Cr_{40}Ti_{60}$ alloy buttons were prepared by melting 99.7% pure Ti and 99.9% pure Cr in argon atmosphere. The enthalpy of the liquid phase was measured using the drop calorimeter. The enthalpy of the β phase at 298 K was taken as zero. The enthalpy of the liquid could be represented by:

$$H^l(T) = -26.3 + 5.10*10\text{-}2\ T \quad \text{kJ/mol} \qquad (3.4)$$

$$H^l(T) = 9.98 + 0.0450T - 3.12*10^4/T \quad \text{kJ/mol} \qquad (3.5)$$

$$C_p^l = (dH^l/dT) \qquad (3.6)$$

The heat capacity of the liquid of the liquid is given by

$$C_p^l = 5.10 \quad \text{J/mol} \qquad (3.7)$$

$$C_p^l = 40.5 + 3.12*10^7/T \quad \text{J/mol} \qquad (3.8)$$

At temperatures less than 700 K, where the β phase was stable for the duration of the measurement, C_p^β was measured directly using the DSC. At T>1400 K, where the β phase could be retained in the dropped sample,

the enthalpy of this phase, Hβ, was measured using the bomb calorimeter.

$$H^{\beta}(T) = -7.17 + 0.0227T + 4.59*10^{-6}\,T^2 \quad \text{kJ/mol} \qquad (3.9)$$

$$C^{\beta}_{p}(T) = 22.7 + 9.18*10^{-3}\,T \quad \text{J/mol.K} \qquad (3.10)$$

C^{l}_{p} has been measured only to limited undercooling. This was extrapolated to lower temperatures. However, this extrapolation would overestimate C^{l}_{p} since the heat capacity of the glass-forming alloys generally increases as undercooling increases due to the decrease in the configurational entropy of the liquid. There was a fairly large uncertainty in ΔH_f (12.0-19.0 kJ/mol) measured by DSC. Considering the uncertainties, the authors calculated the $\Delta G(T)$ for various extreme cases. ΔG (T) increases with temperature and then decreases, after reaching a maximum, in all the cases. The temperature at which ΔG shows a a maximum represents the Kaufman temperature, T_k. Below this temperature, the entropy of the under-cooled liquid becomes smaller than that of the β phase. Though this situation appears paradoxical, it is feasible if the liquid is topologically ordered and β is disordered. Therefore, the liquid may be under-cooled below T_K, but transforms to the glass at the glass transition temperature, T_g. The specific heat is generally larger than that of the corresponding crystalline phase. This investigation showed that even under the most favourable condition, the calculations did not predict spontaneous vitrification of the undistorted $Cr_{40}Ti_{60}$ phase at 873 K. Additional excess free energy of the β phase can make this phase less stable and lead to the formation of the amorphous phase. It is estimated that an additional vacancy concentration of 10^{-3} is required in

the β phase to nullify ΔG=0.4 kJ/mol at 873 K, assuming that the enthalpy of formation of vacancy of the order of 1 eV.

Inverse melting in the Cr-Ti system has been studied by Yuan et.al. using experiments and thermodynamic calculations(11). The authors note that the formation of an amorphous phase from a crystalline phase must be thermodynamically driven and at the same time, the formation of the equilibrium phases has to be kinetically suppressed. The transformation of a crystalline phase has been termed "spontaneous vitrification" , in general. It is called "inverse melting" when a polymorphous transformation occurs. In spite of attempts by different groups, it has not been possible to reproduce the transformation into an amorphous phase, except in one case. Assessment of the thermodynamic driving force for this transformation has produced negative results, in some cases. However, thermodynamic analysis is limited by its critical dependence on models and assumptions. This investigation (11) studied alloys in the Cr-Ti system containing 45-65 at% Cr, produced by mechanical alloying. 99.8 % pure Ti and Cr of particle size less than 300 μm were used in the preparation of the alloys. XRD,TEM and DSC were used in charactersising the alloys during annealing.

$Cr_{40}Ti_{60}$ alloy was studied using DSC and subsequently using XRD after rapid quenching at a rate of 320 K/min. The DSC scan exhibited peaks at 400,500 and 680 °C. When the alloy was held at 400 °C and quenched, the XRD showed sharpening of the original peaks of the alloys, indicating some structural relaxation. The XRD pattern changed dramatically on annealing at 580 C and a diffraction halo appeared at $2\theta = 42°$. The bcc diffraction intensities decreased and the peaks shifted to lower angles.

The position and width of the diffractions halos are in good agreement with amorphisation in Cr-Ti alloys. The concentration of the residual *bcc* phase was estimated to be 23 at% Cr. Therefore, it was inferred that a Cr-rich amorphous phase was formed during the second exothermic peak leading to a decrease in the Cr content of the parent phase. This reaction overlaps slightly with the formation of hcp Ti and $TiCr_2$ at 650 C. Thermodynamic equilibrium is reached at 700 °C.

Isothermal annealing at 650 °C showed that an amorphous phase was formed after 20 minutes leaving a Ti-rich parent phase behind. Traces of α-Ti could be detected after 60 minutes. Complete transformation to the equilibrium phases occurred after 24 hours at 600 °C. A similar result has been reported by a few other investigators with one exception who reported amorphisation. These results showed that solid state amorphisation occurred in $Cr_{40}Ti_{60}$ alloys but the following observations were also made: (a) amorphisation was accompanied by dissociation rather than the process occurring through ploymorphisation as claimed by some investigators; (b) the amorphous phase was formed at lower temperatures and shorter time intervals compared to previous reports. The method of preparation of the alloy adopted in this study could have contributed to the second observation.

In this study, complete amorphisation was achieved only for the $Cr_{55}Ti_{45}$ alloy. Partial amorphisation was observed for other compositions. The first diffraction halos of amorphous $Cr_{50}Ti_{50}$ and $Cr_{55}Ti_{45}$ alloys occurred at 2θ = 41.73° and 42.47 °, respectively. These results are comparable to those observed for alloys produced by sputtering. Diffuse diffraction halos and the lack of image contrast in TEM micrographs of

$Cr_{50}Ti_{50}$ alloy confirmed the presence of an amorphous phase. It was inferred from TEM study that complete amorphisation could be obtained only if the initial alloy was homogeneous on a nanometer scale.

In the case of the $Cr_{45}Ti_{55}$ alloy, the amorphous phase formed at the expense of the bcc phase which exhibited a constant (110) peak position during annealing. For the $Cr_{40}Ti_{60}$ and $Cr_{65}Ti_{35}$ alloys, the peaks shifted to lower and higher diffraction angles, respectively. This observation indicated that the transformation was polymorphous in the case of the $Cr_{45}Ti_{55}$ alloy whereas a decomposition occurred for other compositions. In the final annealed state, the amorphous phase was in meta-stable equilibrium with the bcc phase.

Up to a composition of 50 at%Cr, precipitation of the hcp Ti-rich phase limited the amorphisation reaction. Above this composition, (55-65 at%Cr), $TiCr_2$ was the first equilibrium phase produced on annealing. A time-temperature-transformation diagram of the $Cr_{55}Ti_{45}$ alloy was constructed. Different heating rates, from 5 to 160 K/min., were used in the experiments. The temperatures for the onset of amorphisation and crystallization were determined from the corresponding exothermic peaks. The results showed that slow heating rates or long annealing times at low temperatures favoured amorphisation. This observation is supported by activation enthalpies for amorphisation and crystallizaleation barrier in the Cr-Ti system. reported in literature. These are 2.3 eV for amorphisation and 3.2 eV for crystallization and 2 and 2.7 eV, respectively, for the two processes, as reported by two different investigators.

Phase diagram calculations showed that the driving force for the formation of the amorphous phase from *bcc* phase was about 0.7

kJ/g.atom (at 55 at%Cr), in terms of free energy difference. This is relatively small compared to other systems such as Nb-Co which also exhibit precipitation reaction of the amorphous phase. This can be due to a nucleation barrier in the Cr-Ti system. This can be overcome by introducing a high density of nucleation sites such as grain boundaries and other defects. The meta-stable phase diagram involving the *bcc*, liquid and amorphous phases has been constructed. This diagram predicts a congruent inverse melting at about 746 °C, 55 at%Cr. From the thermodynamic properties of this composition, it has been inferred that the liquid develops a short-range order upon under-cooling. This leads to stabilization of this phase with respect to the crystalline phase. The phase transition at the inverse melting point should be reversible. Such a reversible transformation was reported by other investigators at 30 at% Cr. This observation has been refuted by the authors(11) as thermodynamically impossible, based on the meta-stable phase diagram.

Bormann(12) has discussed the thermodynamic and kinetic requirements for "inverse melting". Since the amorphous phase is thermodynamically the low-temperature state of the under-cooled liquid, solid state amorphisation can be considered as a melting phenomenon. Although amorphisation of super-saturated solid solutions have been observed in Ti- and Nb-based *bcc* alloys, in most cases the super-saturated solution decomposed into a two-phase mixture of an amorphous phase and a less-saturated *bcc* phase. Only in the case of Cr-Ti alloys (at XCr= 0.55), a complete amorphisation of the bcc phase has been observed. This polymorphous transformation can be considered as congruent melting. This is an interesting phenomenon since it requires the

entropy of the amorphous phase to be less than that of the crystalline phase.

In certain systems, such as Nb-Co, Nb-Fe and Nb-Ni, a large difference in stability between the undercooled liquid and the solid solution phases arises out of the large difference in the atomic sizes of the components. These systems provide a large driving force for amorphisation, the formation of extended solid solution being constrained thermodynamically, at the same time.

Solid-state amorphisation has been observed in Ti-Cr, Ti-Mn, Ti-Fe and Ti-Cu systems. Super-saturated solid solutions of $Cr_{40}Ti_{60}$ and $Mn_{25}Ti_{75}$ decomposed into an amorphous phase and a *bcc* phase. $Fe_{40}Ti_{60}$ and $Cu_{60}Ti_{40}$ transformed completely into an amorphous phase. The earlier results of Blatter et.al. on amorphisation has not been confirmed by any other group, though several investigations have been carried out by other research groups. Thermodynamic calculations show that a driving force for amorphisation exists in the Cr-Ti system, only if the *bcc* phase is completely disordered. It appears that a small amount of B2 ordering in the *bcc* structure can prevent amorphisation. The thermodynamic driving force for amorphisation is less than 1 kJ/g.atom at temperatures where the transformation is feasible kinetically. Hence, there would be a high activation energy for homogeneous nucleation. This possibly explains that the transformation has not been detected in many of these alloys. The entropy of fusion of the $Cr_{0.55}Ti_{0.45}$ alloy is about 3.5 J/g.atom. which is relatively small compared to other alloy systems. The liquid, therefore, has a small configurational entropy resulting from an increased level of chemical short-range order. Inverse Melting is a first-order transformation

with an exothermic heat of fusion of 5 kJ/g.atom. and a negative entropy of 5 J/g.atom. At temperatures less than that of Inverse Melting, the amorphous phase is stabilized by its chemical order. Disordering in the crystalline phase increases its free energy, making the transformation to the amorphous phase more likely. Since Inverse Melting is driven by chemical ordering in the liquid phase, only those systems that have a negative heat of mixing can exhibit the Inverse Melting phenomenon. Similarly, Inverse Melting is favoured in alloys where the entropy of fusion is small.

Polymorphous transformation of a homogeneous meta-stable phase is only one case of Inverse Melting. Other cases such as the formation of an amorphous through a peritectic reaction are also possible. These would involve transformation of a multi-phase crystalline structure into an amorphous phase. The possibility of such a transformation in the Nb-Al alloys has been predicted based on thermodynamics.

Blatter et.al.(13) have discussed spontaneous vitrification in the Cr-Ti alloys in the composition range 15 to 55 at% Cr. The β phase can be retained by slow cooling, at about 100 K/s, from its equilibrium temperature. This phase can not decompose spinodally since there is no coherent spinodal. $Cr_{40}Ti_{60}$ alloy has been prepared by melting pure chromium and titanium in a vacuum furnace. The melted alloy which contained Cr_2Ti and α-Ti phases, was cut into cubes, about 5mm wide. The cubes were heated in argon atmosphere at a temperature where β was the stable phase, for several seconds. The cubes were then quenched in water. The quenched samples were covered with a layer of oxide and equilibrium phases. The layer was removed by polishing to expose the β

phase. The β cubes were annealed in a high vacuum furnace at 600 °C for periods ranging from several hours to several days. Slices made from the annealed samples were studied using XRD to confirm vitrification. In addition to the halo characteristic of the amorphous phase, some extra weak diffraction lines, designated as β′ and ω, appeared. Spontaneous vitrification was non uniform on a macroscopic scale. It started preferentially at grain boundaries and on the surface. There was always a sharp boundary between the β phase and the amorphous region. The velocity of the boundary was about 1^{-10} μm/hr during annealing. Energy dispersive x-ray microanalysis with a spatial resolution of about 1μm showed that there was no difference in the composition between the amorphous and crystalline regions. This showed that the movement of the β-amorphous boundary did not involve any macroscopic large-scale mass transport. Bulk vitrification was achieved in the range 55-65 at% Ti. This range is significantly smaller than that observed in thin films.

TEM studies of the samples confirmed the presence of a web-like superstructure of the β phase. The relevance of the superstructure in the parent β phase on the occurrence of spontaneous vitrification was not clear. The vitrified phase is homogeneous down to a scale of 10 A or less. However, there was evidence of scattered inclusions embedded in the vitrified matrix. The crystalline inclusions had grain size around 30 A. The crystalline inclusions were interpreted by the authors(13) to consist of a *bcc* solid solution of approximate composition$Cr_{10}Ti_{90}$. The authors surmised that this phase was in equilibrium with the amorphous phase. This phase could be found in both bulk and thin samples and did not disappear after a very long annealing at 600 °C. The volume fraction of

the crystalline phase in the spontaneously vitrified material was about a few percent.

The appearance of the ω phase was considered by the authors to be somewhat disturbing because it did not fit into the picture of the picture of the simple β-amorphous equilibrium. This phase is known to be a meta-stable transition structure between the β phase (bcc) and the α phase (hcp). The authors suggested a reaction model which consisted of a two-stage reaction : (a) $\beta \rightarrow \alpha + \beta'$ and $\beta' \rightarrow \beta' + \omega$. The second reaction occurred inside the β' phase and appeared to occur below 600 °C during the cooling of the samples after furnace annealing.

Greer(14) has discussed the thermodynamics of Inverse Melting. He has proposed that "Inverse Melting occurs on cooling a crystal because the system can lower its overall entropy by chemical ordering", when the liquid is formed. A liquid can be chemically ordered when the crystal is not, when the atomic coordination numbers in the two phases are significantly different. The coordination number in alloy liquids and glasses, i.e. 11-12, is close to that in close-packed crystals and is significantly higher than that in *bcc* crystals where it is 8. In addition, the *bcc* crystals generally have a higher vibrational energy compared to the close-packed systems. This also favours Inverse Melting.

In the case of the Cr-Ti system, the β phase has a large positive regular solution parameter. The liquid has a small positive parameter. Therefore, there is no distinct tendency for ordering in the liquid. But, the difference in the interaction parameters is consistent with the model for Inverse Melting. The following expression was used for calculating the free energy difference between the liquid and crystal phases:

$$\Delta G(T) = \Delta S(T_m)(T_m-T)-[\Delta Cp(T_m)(T_m-T)^2](1-((T_m-T)/6T)) \qquad (3.11)$$

For glass-forming liquids, ΔC_p is positive and significant. The specific heat of the liquid can be almost twice that of the crystal near T_g. ΔG increases less rapidly on cooling. For glass-forming systems, ΔC_p between the crystallization temperature and T_m is about $0.8\Delta(T_m)$. This value was assumed for the $Cr_{30}Ti_{70}$ alloy. The $\Delta G(T)$ vs T plot indicated some topological ordering in the liquid, as it cooled. $\Delta G(T)$ reached a maximum at 775 K. The liquid and crystal are iso-entropic at this temperature. This is less than the temperature at which amorphisation has been observed in this system (873 K). $\Delta G(T)$ is not expected to become zero at any reasonable temperature.

In the next step of modeling, it was assumed that at low temperatures, the crystal retained its entropy of chemical order but the liquid did not. The liquid was assumed to order completely at a critical temperature, T_c. It was found that when T_c was equal to T_m, $\Delta G(T)$ became zero at the temperature interval where reversible amorphisation has been observed. A meta-stable phase diagram developed on the basis of this model showed that a meta-stable liquid existed in the range 40-50 at % Cr, with a congruent Inverse Melting occurring at about 1400 K for the composition $Cr_{50}Ti_{50}$. However, this model suffers from the major draw-back that it assumes ordering in the liquid phase close to its melting temperature, in spite of the fact that the regular solution parameter is positive.

4. Transformation Diagrams

4.1 Introduction

Equilibrium phase diagrams predict the composition ranges of various phases that can exist in a system at equilibrium. However, real processes deviate significantly from equilibrium. Several models have been used to predict the progress of phase transformation in these cases. A common approach is to assume equilibrium at the interface between the phases across which phase transformation occurs. For example, when a liquid solidifies, it is assumed that the liquid and solid are at equilibrium at the interface between the two. Equilibrium phase diagrams are used for predicting the composition of the solid at the interface given that of the liquid. The same approach is sued for studying solid-solid transformation also. However, the model still assumes equilibrium at the interface. The interface, in most cases, would be at meta-stable equilibrium and not correspond to the equilibrium predicted on the basis of the phase diagram. Conventional approaches can not predict from first principles which stable and meta-stable equilibrium phases can be assumed to be present at the interface and the composition range of the co-existing phases in the latter case. For example, during the solidification of steel, the austenite phase is sometimes formed in a composition range where ferrite and liquid are the equilibrium phases. The formation of the austenite is explained by the construction of a meta-stable extension of the (austenite+liquid) field into the (ferrite+liquid) region. The compositions of the austenite and liquid phases are inferred from the meta-stable phase boundaries. This empirical approach gives the composition of the phases as if the austenite and liquid were at equilibrium at the interface, instead of the ferrite and liquid

phases. This model does not explain why the austenite phase is formed in preference to the ferrite phase. A quantitative technique based on the principles of stability of non-equilibrium phases is required for this purpose. Also, in the conventional approach, the composition of the solid that is formed at the interface is predicted when the liquid reaches the liquidus temperature. This approach is not sufficient to predict the composition of the solid below the liquidus temperature of the composition. A tool that is based on the principles of phase stability can be readily adopted to address the equilibrium as well as non-equilibrium phase transformation simultaneously. The transformation diagrams can be readily adopted for this purpose. They also can address the questions mentioned above for modeling phase transformation during the processing of alloys.

4.2 Transformation Diagrams

Uni-directional transformation diagrams have been used to study the process of rapid solidification[15]. These diagrams are used to infer the range of solid composition that can form when the liquid solidifies under non-equilibrium conditions. These diagrams are 'uni-directional' since they explore phase transformation in only one direction i.e. from the liquid to the solid, and not in the revere direction. Usually these diagrams are used to predict the possible solid composition during rapid solidification. Some attempts have been made to study non-equilibrium melting using the free energy-composition diagrams(16,17). The utilization of these diagrams to model other non-equilibrium phase transformation, remains unexplored. For example, application of these diagrams under conditions when more than one solid can form from the liquid has not been studied. Under normal conditions, phase transformations are not uni-directional. Transformation in one direction is always accompanied by transformation

in the opposite direction also, though these two would proceed at different rates. It is the net result of these two rates that determines the overall direction of phase transformation. This aspect of phase transformation has to be taken into consideration for developing a realistic model of phase transformation during the processing of alloys. These diagrams do not address the case where the parent and the daughter phases co-exist. For example, the diagrams can tell what would be the composition of the solid that forms from a liquid but can not predict the conditions under which both the solid and liquid phases are stable. Information on the simulateneous stability of more than one phase is essential for studying the phenomenon of phase transformation.

4.3 Construction of Transformation Diagrams

Fig.4.1 represents the free energy-composition diagram of a hypothetical system A-B at a temperature 'T'. The transformation of alloy X_B^{β} from the 'β' phase to the 'α' phase is considered. This transformation can be considered to occur in two steps: (1) fluctuation of the composition of the alloy from X^{β} to X^{α} without a phase change and (2) transformation of the alloy of composition X^{α} from the 'β' phase to the 'α' phase. The free energy change accompanying the second step is called the 'transformation free energy change'. This is given by:

$$\Delta G^{\alpha\beta} = X^{\alpha}_{A}\Delta\mu_A + X^{\alpha}_{B}\Delta\mu_B \qquad (4.1)$$

Where $$\Delta\mu_i = \mu^{\alpha}{}_i\mu^{\beta} \qquad (4.2)$$

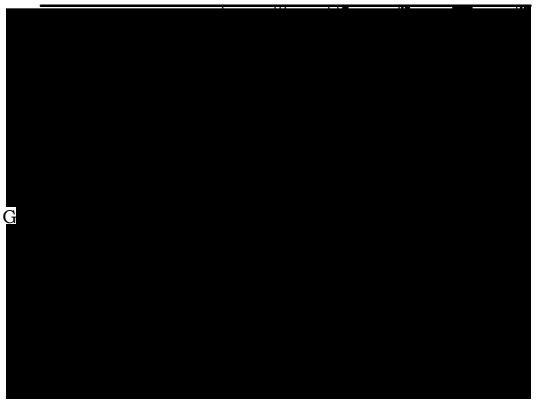

Fig. 4.1 Free Energy - Composition Diagram

Here X_i, is the atom fraction and μi,, the chemical potential of the component 'I'. X^{α}_B in the 'β' phase can transform to X^{α}_B in the 'α' phase, when $\Delta G^{\alpha\beta}<0$. A tangent to the G^{β} line at X^{β}_B cuts the G^{α} line at the points `P' and 'Q'. At these two points, $\Delta G^{\alpha\beta}$ =0. At all compositions lying between 'P' and 'Q', $AG^{\alpha\beta}<0$. Different compositions of 'P' and 'Q' are obtained for different compositions of X^{β}_B. Mapping the points that satisfy the equality $\Delta G^{\alpha\beta}=0$ on the composition-composition space, generates the transformation diagram, fig.4.2. The line AMEB in the figure is the locus of the point satisfying the condition $\Delta G^{\alpha\beta}$ =0. A line perpendicular to the X^{β}_B-axis will cut the locus at the points `P' and 'Q'. Transformation from the '$\beta$' to the '$\alpha$' phase is possible for all the compositions lying between P and Q i.e. if the composition of the alloy in the `β' phase fluctuates to any composition in this range, the transformation to the 'α' is favoured thermodynamically. A tangent to the $\Delta G^{\alpha\beta}$ =0 line parallel to the X^{α} -axis meets the line at the point 'E'. This represents the equilibrium composition at the temperature considered. The point 'M' represents the highest value of X^{α}_B which satisfies the condition $\Delta G^{\alpha\beta}$ =0. At this point G^{α} = G^{β}. It is also referred to as the massive transformation point.

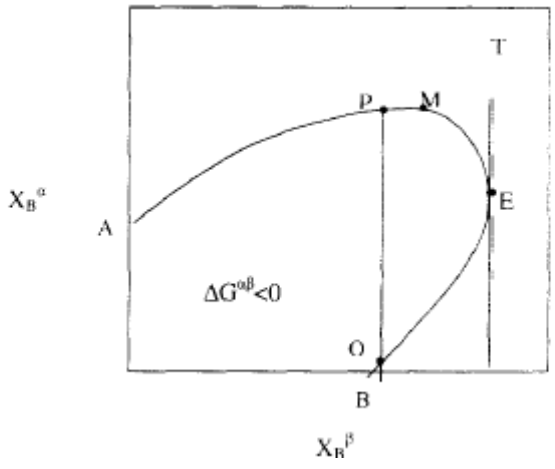

Fig. 4.2 Transformation Diagram

The following expression gives the transformation free energy change when transformation from the `α' phase to the β phase occurs:

$$\Delta G^{\beta\alpha} = -(X^{\beta}_{A}\Delta\mu_A + X^{\beta}_{A}\Delta\mu_B) \qquad (4.3)$$

When $\Delta G^{\beta\alpha} < 0$, an alloy of composition X^{β}_{A} in the 'α' phase can transform to the 'β' phase of the same composition. The compositions at which

$\Delta G^{\beta\alpha} = 0$, are given by the intersection of the G^{β} by tangents to the Gαline in the free energy-composition diagram. Fig.4.3 shows the two sets of loci of points which satisfy the conditions $\Delta G^{\beta\alpha} = 0$ and $\Delta G^{\alpha\beta}=0$. The curve $\Delta G^{\alpha\beta}=0$ is concave towards the origin whereas the curve $\Delta G^{\beta\alpha} = 0$ is convex towards it. This results from the fact that 'α' is the stable phase when $X_B \rightarrow 0$. The equilibrium point is given by the intersection of the $\Delta G^{\beta\alpha} = 0$ and $\Delta G^{\alpha\beta}=0$ lines. These two lines also intersect at the point `M' where $G^{\alpha} = G^{\beta}$. The two points `E,' and `M' are distinguished by the fact that the tangents to the two lines $\Delta G^{\alpha\beta} = 0$ and $\Delta G^{\beta\alpha}=0$ and parallel to the X^{α} and X^{β}

axes, respectively, intersect at the equilibrium point. Tangents to the $\Delta G^{\alpha\beta}$ = 0 and $\Delta G^{\beta\alpha}$=0 lines and parallel to the X^{β} and X^{α} axes intersect at the point M.

4.4 The Bi-Directional Transformation Diagram

The region enclosed by the curve $\Delta G^{\alpha\beta}$ =0 in fig.4.2 gives the compositions which thermodynamically favour phase transformation from the 'β' phase to the `α' phase. If any alloy of composition X^{β}_{B} in the β-phase fluctuates in composition to a composition lying within this region, phase transformation from the 'β' to the 'α' phase is possible. However, this figure does not inform if this alloy in the 'α' phase can undergo a phase transformation to the `β' phase through fluctuations in composition. This information is crucial for modeling phase transformations during the processing of alloys. This question can be addressed by the bi-directional transformation diagram given in fig.4.3.

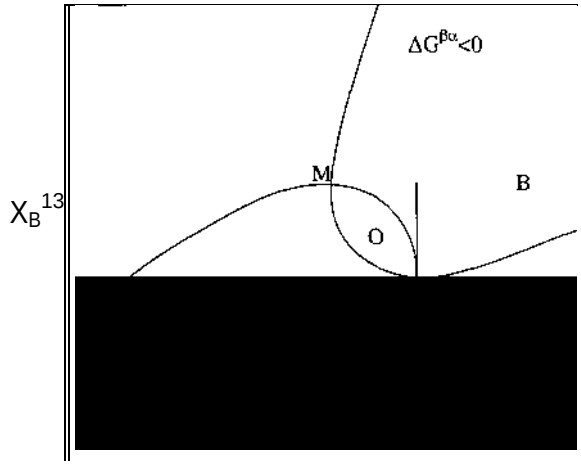

Fig. 4.3 Transformation Diagram — Forward and Backward Phase Transformation Reactions.

Fig.4.3 has three significant regions. In region A, transformation from 'β' to`α' phase is possible thermodynamically. However, the reverse transformation is not possible. In region 'B", when an alloy with the `α' phase structure fluctuates to a composition along the horizontal axis in this region, phase transformation from the 'α' to the 'β' phase is possible. A fluctuation in composition of an alloy with the 'β' phase structure to any composition lying along the vertical axis within this region does not favour a phase transformation. In the region 'C', both the phase transformations are possible. If an alloy with the 'β' phase structure fluctuates in composition along the vertical axis within this region, phase transformation from the 'β' to the 'α' phase is possible. On the other hand, if an alloy with a structure of the 'α' phase whose composition lies within this region fluctuates in composition along the horizontal axis, phase transformation from the `α' to the 'β' phase is possible. Therefore, the bi-directional transformation diagrams show that there are regions of compositions where both the $\alpha \rightarrow \beta$ and $\beta \rightarrow \alpha$ transformations are possible. Introduction of this region facilitates a systematic modeling of phase transformation during the processing of alloys. This region is a representation of the region bounded by the equilibrium compositions, $X^{\alpha,e}_B$, $x^{\beta,e}_B$ and the massive transformation point 'M' in the free energy-composition diagram, fig. 4.1.

Let us consider an alloy undergoing a phase transformation from the 'β' phase to the `α' phase. Initially there would be only the 'β' phase. This would be followed by the formation of the `α' phase with an interface between the two. The latter would grow at the expense of the former until the transformation is complete. The final structure might have only the 'α' phase or a mixture of both the phases depending on the thermodynamic nature of the system and the kinetics of phase transformation. The conventional representation of transformation diagrams as given in fig.4.2 does not allow for the presence of both the phases. This implies the transformation to be uni-directional and does not assist development of a model to explore phase transformation in metallurgical processes. This figure is useful to study cases where transformation is extremely rapid.

Fig.4.4 shows the free energy-composition relation at a temperature 'T'. The G^{α} and the G^{β} lines do not meet at any point. Tangents to the G^{β} line would not intersect the G^{α} line. But, tangents to the G^{α} line would intersect the G^{β} line. Therefore, in the transformation diagram, the $\Delta^{\beta\alpha}$ =0 line would be present but the$\Delta^{\alpha\beta}$=0 line would be absent.

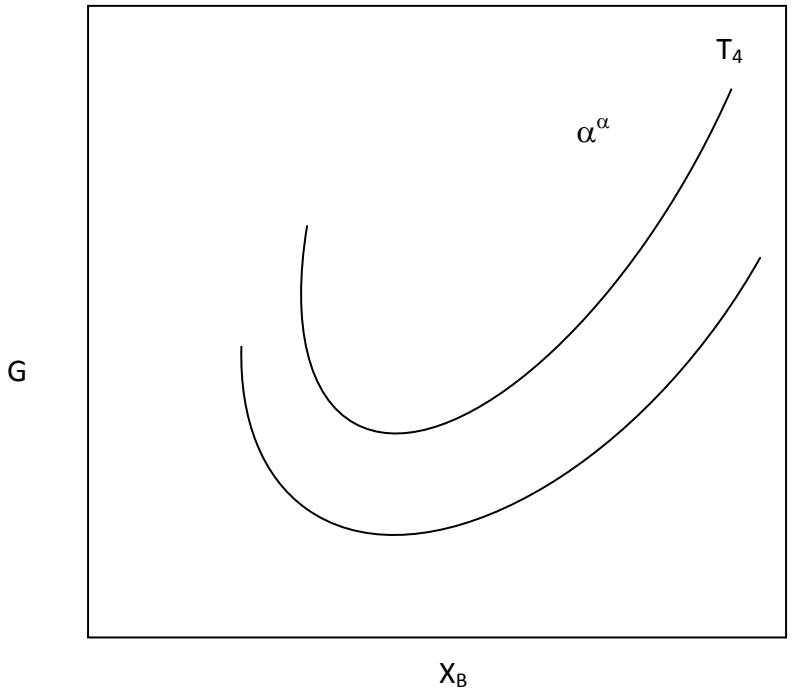

Fig. 4.4 Free energy – Composition Diagram (The free energy lines do not meet)

5. Thermodynamics of Inverse Melting

Investigations carried out by various groups have shown that the *bcc* phase transforms to the amorphous on annealing at low temperatures. This phenomenon has been observed in several titanium binary alloys and also in some other alloys such as niobium binary systems. The following observations have been made:

(a) the formation of the amorphous phase from the *bcc* structure occurs ahead of transformation to the equilibrium phases, since the latter process is sluggish due to the low diffusivity of atoms in the matrix.

(b) The *bcc* phase is made les stable compared to the amorphous phase due to the concentration of defects in the quenched *bcc* structure.

(c) The amorphous phase is formed when the *bcc* structure retained by laser quenching or water quenching is annealed. This phase is not formed if the β phase retained from high temperature by splat-cooling is annealed. This is attributed to the absence of defects in the latter samples.

(d) The free energy difference between the *bcc* structure and the amorphous phase must be about 8 J/mol for the transformation to be possible thermodynamically.

(e) The amorphous phase is always interspersed with fine particles of a *bcc* phase whose composition is different from that of the parent *bcc* phase.

(f) The ω phase is observed to be associated with the amorphous phase. This phase might be formed either during the quenching of the parent β (bcc) phase or during the subsequent annealing.

(g) Thermodynamic models have been constructed to rationalize the formation of the amorphous phase. These models have assumed that the amorphous phase is formed directly from the β phase. Free energy-composition diagrams constructed based on the models show that the free energy of the β phase, made less stable due to the presence of defects, to be higher than that of the amorphous phase. A meta-stable phase diagram, constructed based on this model indicates a congruent, reversible transformation between the βphase and the amorphous phase in the Ti-Cr system at a composition of 55 at% Cr.

However, this model is inconsistent with an experimental observation of a polymorphous transformation of the β phase at X_{Cr}=0.3 (X_{Cr}-atom fraction of Cr) in the Ti-Cr system.

(h) The thermodynamic models suffer from low accuracy of the various thermodynamic data used in the construction of the models. Some calculation, in fact, show that the β phase is more stable compared to eth amorphous phases except at extremely low temperatures.

(i) The thermodynamic models predict topological ordering in the liquid at low temperatures leading to its enhanced stability. Hence, "SV" is observed mostly systems where the liquid exhibits a negative enthalpy of mixing.

(j) These models can not explain the observation of the appearance of the ω phase during annealing except as the appearance of an equilibrium *hcp* phase which is followed by the formation of the non-equilibrium amorphous phase.

The thermodynamic models attempted so far have always treated the formation of eth amorphous phase as an equilibrium phenomenon between two meta-stable phases, viz., the quenched β phase and the amorphous phase. The traditional tool of constructing equilibrium phase diagram, i.e. computing the Free energy-Composition relation in each phase and constructing a common tangent between the two phases, has been always used in predicting the formation of the amorphous phase form the *bcc* phase. However, the transformation process itself is a non-equilibrium process apart from the fact that the phases under consideration are meta-stable phases.

Let us consider fig. 5.1 where M_1 and M_2 are two meta-stable phases. The free energies of the phases are given as functions of composition. In the region "A", the phase "M_1" is stable and in the region "C", the phase "M_2" is stable. If an alloy of composition in the region "A" and structure of M_2 is held at the temperature T, the phase will transform to the structure M_1. A similar phenomenon will occur in the region "C", structures M_1 and M_2 playing a reverse role. In the region "B", an alloy in the structure M1 will transform to a mixture of the structures M_1 and M_2 whose

compositions are given by the "equilibrium" compositions M_1^e and M_2^e. However, since the transformation process itself is a non-equilibrium process, analysis of phase transformation based on this approach can be erroneous. There are systems where transformation from structure M_1 to structure M_2 is possible but the reverse is forbidden thermodynamically. Therefore, the approach used conventionally for studying non-equilibrium phase transformation will not be valid in many cases.

The Transformation Diagrams have been successful in modeling the thermodynamics of non-equilibrium phase transformation as demonstrated in a previous chapter. The Transformation Diagrams were used for interpreting the process of spontaneous vitrification in titanium-binary alloys.

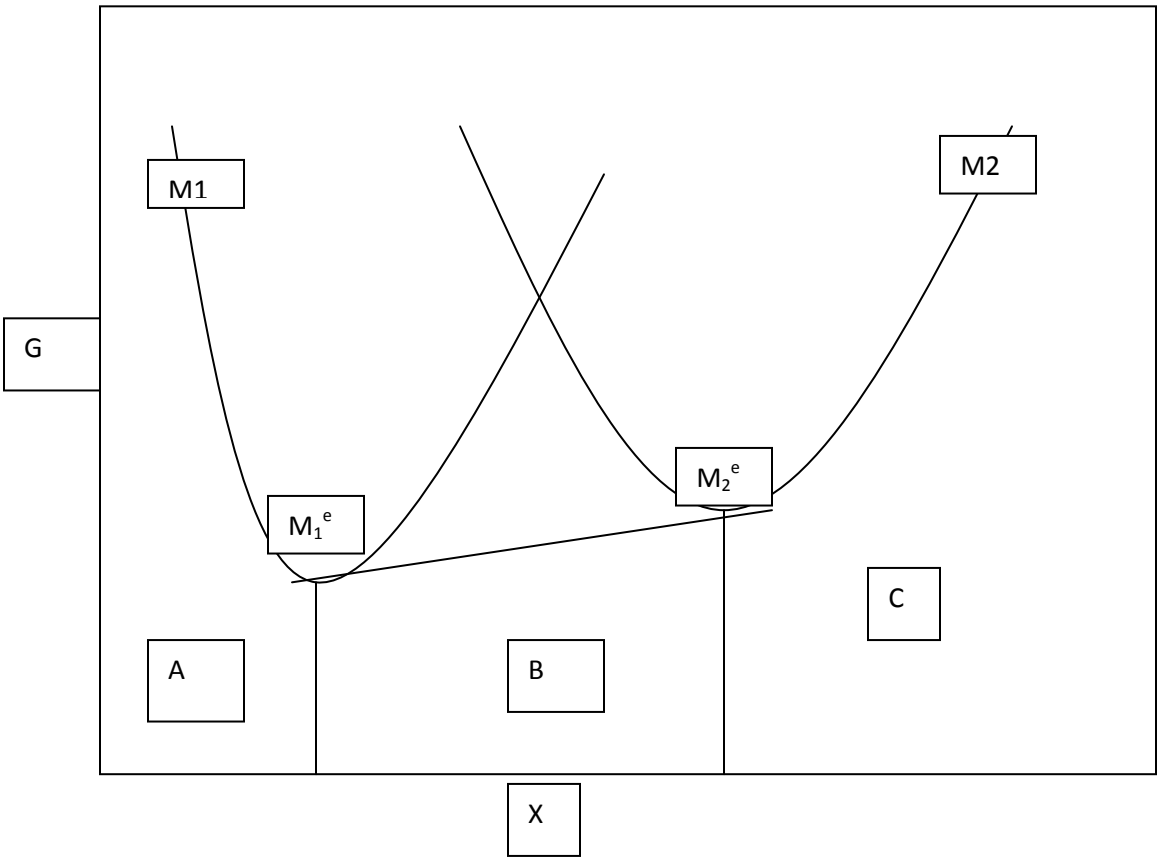

Fig. 5.1 Free Energy-Coposition Diagram for Meta-stable Phases

6. Transformation Diagrams for Titanium-Binary Systems

6.1 Introduction

The transformation diagrams were constructed for the Cr-Ti system. The relevant data were obtained from published literature(18-20). The Cr-Ti phase diagram(21) is given in figure 6.1. Figure 6.2 gives the bi-directional transformation diagram for this system at 1773 K. The axes of the diagram represent the atom fraction of chromium in the liquid(l) and the b.c.c.(β) phase. The line GSM1 is the locus of the point satisfying $\Delta G^{\beta l} = 0$. Within the regions enclosed by this line, transformation from the liquid to the b.c.c phase is favoured thermodynamically. In other words, if a liquid whose composition is represented on the x-axis fluctuates in composition along the vertical axis within the region enclosed by this line, then the free energy change for the phase transformation from the liquid to the solid phase is less than zero.

The line GLM which forms a closed loop is the locus of the point satisfying the condition $\Delta G^{l\beta} = 0$. If the solid phase whose composition is given by the vertical axis fluctuates in composition along the horizontal axis within the region enclosed by this line, then phase transformation from the solid to the liquid state is favoured thermodynamically. The regions enclosed by GSM1 and GLM overlap in a region where transformation to both the liquid and solid phases are favoured thermodynamically through fluctuations in the composition of the solid and liquid phases, respectively. This is the region where both the liquid and solid phases co-exit in the phase diagram. If this region is absent in the transformation diagram, then the temperature-composition phase diagram will not show any region where the solid and liquid co-exit. This is true irrespective of whether a pair of stable or meta-stable phases in considered. The line GSM2 and its intersection with the line GLM also can be interpreted in a manner similar to the above.

Figure 6.3 represents the transformation diagram for the β-L pair of phases at 873 K. In this figure, the locus $\Delta G^{\beta l} = 0$ is split into two segments. The first segment extends from $X_{Cr}^{l} = 0$ to $X_{Cr}^{l} = 0.08$ where X_{Cr}^{l} is the atom fraction of chromium in the liquid phase. At, say, $X_{Cr}^{l} = 0.05$, the liquid can transform to any solid whose

composition lies between $X_{Cr}^{\beta} = 0$ and $X_{Cr}^{\beta} = 0.53$. A similar interpretation is valid for the other liquid compositions lying within the range given above. The composition of the solid that can form from a liquid of a given composition is given by the line $\Delta G^{\beta l} = 0$. The other part of the locus $\Delta G^{\beta l} = 0$ extends from $X_{Cr}^{l} = 0.65$ to $X_{Cr}^{l} = 1.0$. At, say, $X_{Cr}^{l} = 0.7$, the liquid can transform to any solid whose composition lies between $0.05 < X_{Cr}^{l} < 1.0$. At $0.08 < X_{Cr}^{l} < 0.6$, the liquid can transform to any solid composition.

The locus $\Delta G^{l\beta} = 0$ is absent at this temperature. In other words a liquid present at this temperature can transform to a solid with the b.c.c structure but transformation in the reverse direction is not possible. No solid in the b.c.c phase can transform to the liquid phase, irrespective of the composition of the solid phase. The free energy change $\Delta G^{l\beta}$ is always greater than zero, for any pair of solid and liquid compositions chosen. Therefore, liquid can not form from the b.c.c. phase at this temperature.

Figure 6.4 is the transformation diagram for the β/α pair of phases, at 873 K. This figure shows that the b.c.c. (β) phase in the composition interval $0 < X^{\beta}_{Cr} < 0.21$ can transform to the α (h.c.p.) phase. The h.c.p. phase in the composition interval $0 < X^{\alpha}_{Cr} < 0.2$ can transform to the b.c.c phase. This figure shows the truncated locus of $\Delta G^{\beta\alpha} = 0$. The upper composition limit of the h.c.p. that can transform to the b.c.c phase can extend beyond $X^{\alpha}_{Cr} = 0.2$. Figure 6.5 gives the $\Delta G^{\alpha\beta} = 0$ at the same temperature but in a different composition range. The b.c.c. in the composition interval $0.585 < X^{\beta}_{Cr} < 0.96$ can transform to the α phase.

Figure 6.6 shows that at 873 K, the liquid phase in the composition interval $0.0 < X^{l}_{Cr}, < 1.0$ can transform to the α phase. At $X^{l}_{Cr} = 0.1$, for example, the transformed solid can have a composition in the range $0 < X^{\alpha}_{Cr}, 0.325$. Above this composition, the liquid-to-h.c.p. phase transformation is not favoured thermodynamically, at this liquid composition. There are two regions covered by the locus $\Delta G^{l\alpha} = 0$. The first region extends from $0 < X^{l}_{Cr} < 0.525$ and $0.56 < X^{\alpha}_{Cr} < 1.0$. In this region, the h.c.p. phase can transform to the liquid phase through fluctuations in the composition of the solid phase. For example, let us consider an alloy $X^{\alpha}_{Cr} = 0.7$. When there are local fluctuations in the

composition of the alloy, the h.c.p. phase can transform to the liquid phase. This transformation is favoured if the fluctuation is restricted to $0<X^{l}_{Cr}<0.45$, at this composition of the h.c.p. phase. The other parts of this region also can be interpreted in a similar manner. The h.c.p. phase can transform to the liquid phase again in the composition interval $0.055< X^{\alpha}_{Cr}<0.27$ as seen from the right, bottom corner of this figure.

6.2 Crystalline-to-amorphous Phase Transformation

Comparison of figure 6.3 with figure 6.6 highlights a remarkable feature. Whereas an h.c.p.-to-liquid transformation is possible at 873 K, the b.c.c.-to-liquid transformation is forbidden. From the arguments above it is seen that the b.c.c-to-liquid transformation is not possible at 873 K. Hence, the b.c.c. phase retained on quenching can not transform directly to the amorphous phase at this temperature. On the other hand, it can transform to the h.c.p. phase. This phase a maximum solubility of 1 at% Cr at 873 K. Hence, an alloy whose composition is greater than 1 at.% Cr will tend to transform to the stable state which is a mixture of h.c.p. and $TiCr_2$ phases. The alloy would tend to precipitate the $TiCr_2$ intermetallic phase from the super-saturated h.c.p. phase. However, this would require large fluctuations in composition. When fluctuations occur in the h.c.p. phase, a situation might arise in certain composition ranges where transformation to the liquid state is favoured thermodynamically. Therefore, instead of forming the stable, equilibrium phase, $TiCr_2$, the alloy would form the meta-stable liquid phase. This leads to the phenomenon of inverse melting. This occurs through the following steps in the Cr-Ti system:

$$\text{b.c.c} \rightarrow \text{h.c.p.} \rightarrow \text{liquid} \qquad (6.1)$$

The b.c.c phase initially transforms to the h.c.p. phase which, in turn, transforms to the liquid phase.

The thermodynamic model reported earlier(14) to describe inverse melting in the Cr-Ti system required the liquid to be highly ordered at a temperature close to T_m, the melting temperature of the alloy. This assumption was not consistent with the

interaction parameter in the liquid. It is known that on annealing at low temperatures, the b.c.c structure in the Cr-Ti system decomposes into two different b.c.c solid solutions, one rich in chromium and the other rich in titanium(22-26). Blatter et.al.(13) observed in the annealed samples, a b.c.c phase with a composition $Cr_{10}Ti_{90}$. The other product of decomposition would have been rich in chromium. Figure 5 shows that a b.c.c phase rich in chromium can transform to a h.c.p phase containing up to 1.8 at% Cr. Figure 6 shows that this h.c.p. phase would transform to aliquid rich in chromium (~45 at%Cr). This would bring the liquid phase close to the same composition as the original alloy which contained 40 at % Cr. Therefore, one would observe that the liquid phase formed on annealing would not differ from the parent phase in composition. This, indeed, has been observed to be the case(13,14). In the region where the $\Delta G^{\alpha l}=0$ and the $\Delta G^{l\alpha}=0$ loci intersect, the transformation would be reversible. The same is true of the intersection between the $\Delta G^{\beta l}=0$ and the $\Delta G^{l\beta}=0$ loci. Therefore, $\beta\rightarrow$ liquid transformation would be reversible.

It has been discussed in detail in reference 27, how the nature of the free energy-composition diagrams control the formation of meta-stable phases. In the Cr-Ti system, at 873 K, the h.c.p. structure is the stable phase up tp 5 at% Cr. (fig. 6.7). At higher levels of chromium, the b.c.c structure is more stable. The liquid is the least stable phase. The free energy-composition line of the h.c.p. phase lies in between the lines of the b.c.c and the liquid phases. The relative curvatures of the free energy lines of the h.c.p. and the liquid phases allow construction of tangents to one line intersecting the other, which is required for the desired transformation to occur(27). This is not possible in the case of the b.c.c.-liquid pair. Hence, the h.c.p. structure transforms to the liquid and the b.c.c structure does not.

It has been demonstrated earlier[11] that the composition axes in the transformation diagrams can be transformed to the chemical potentials. The free energy of a system is given by(28)

$$G = \sum X_i \mu_l \qquad (6.2)$$

μ_i is the potential term and X_i, the co-efficient. There is no distinction between the various potential terms such as the chemical potential, temperature, pressure etc. The transformation diagrams can be constructed with different potential terms along the axes. Therefore, the concepts discussed here can be extended to other systems such as polymers and super conductors where temperature, pressure and applied magnetic fields play the role analogous to that of the chemical potentials in the case considered here.

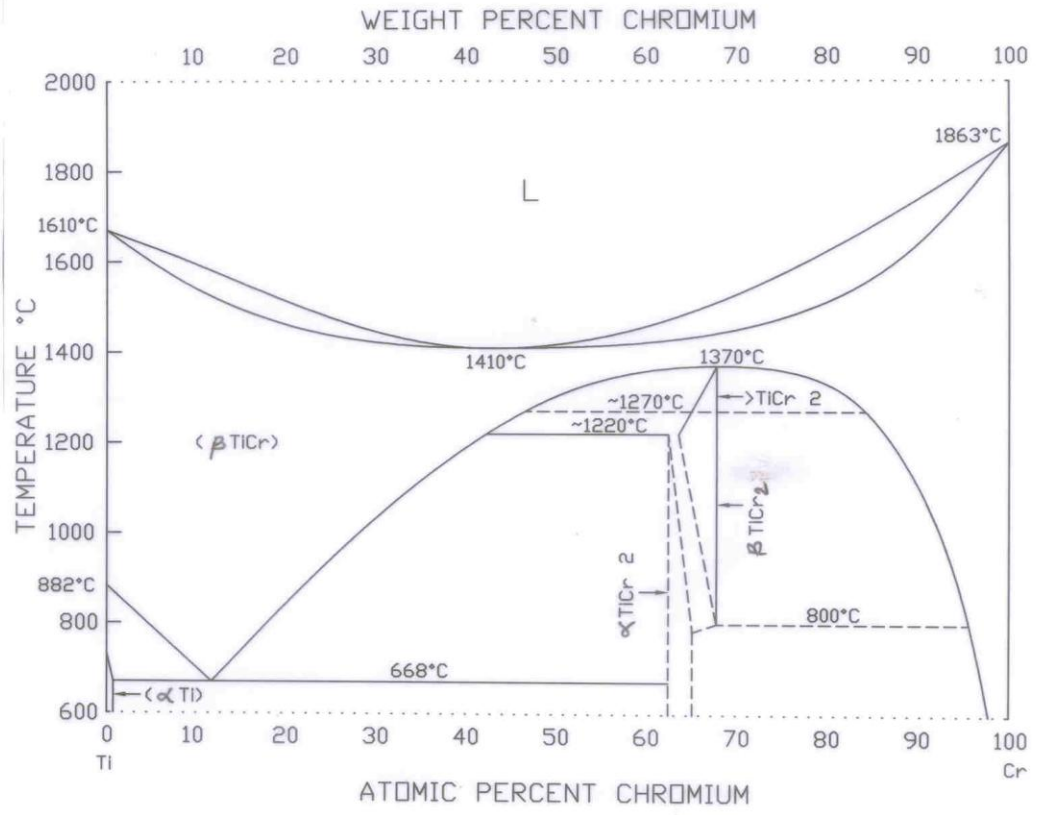

Fig. 6.1 The Ti-Cr Phase Diagram (10)

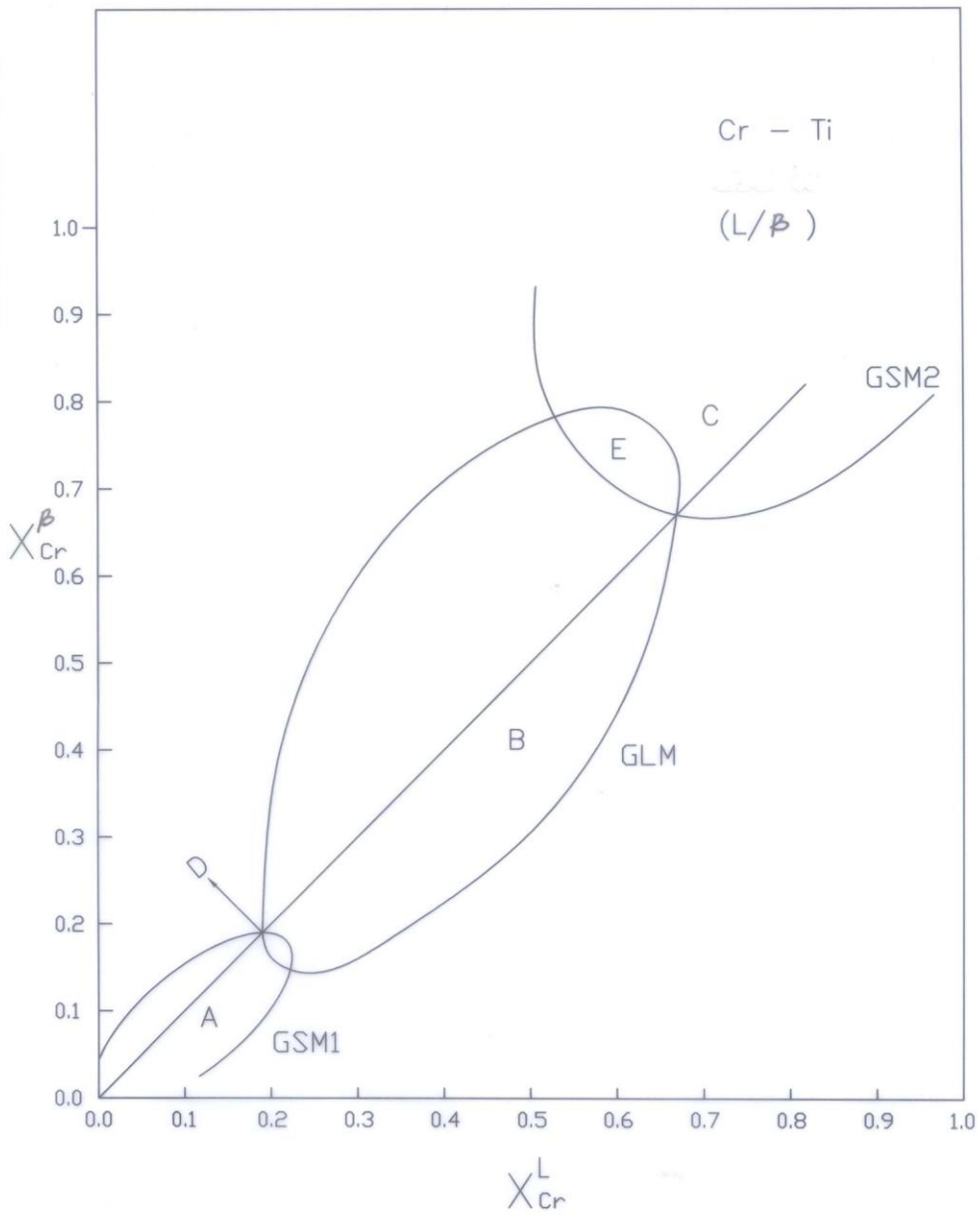

Fig. 6.2 Transformation Diagram of the Ti-Cr System at 1773 K

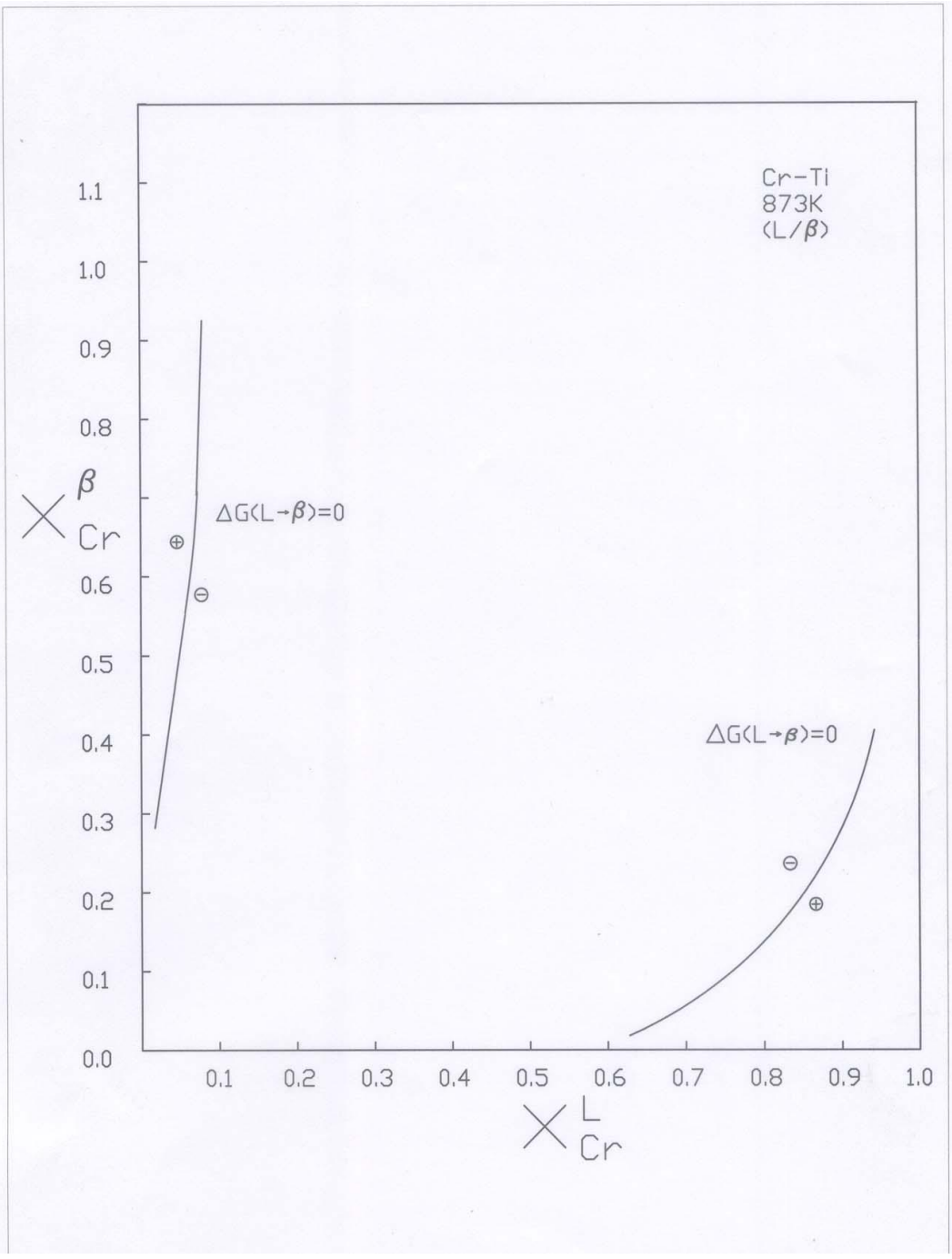

Fig. 6.3 The L/β Region of the Transformation Diagram of the Cr-Ti System at 873 K

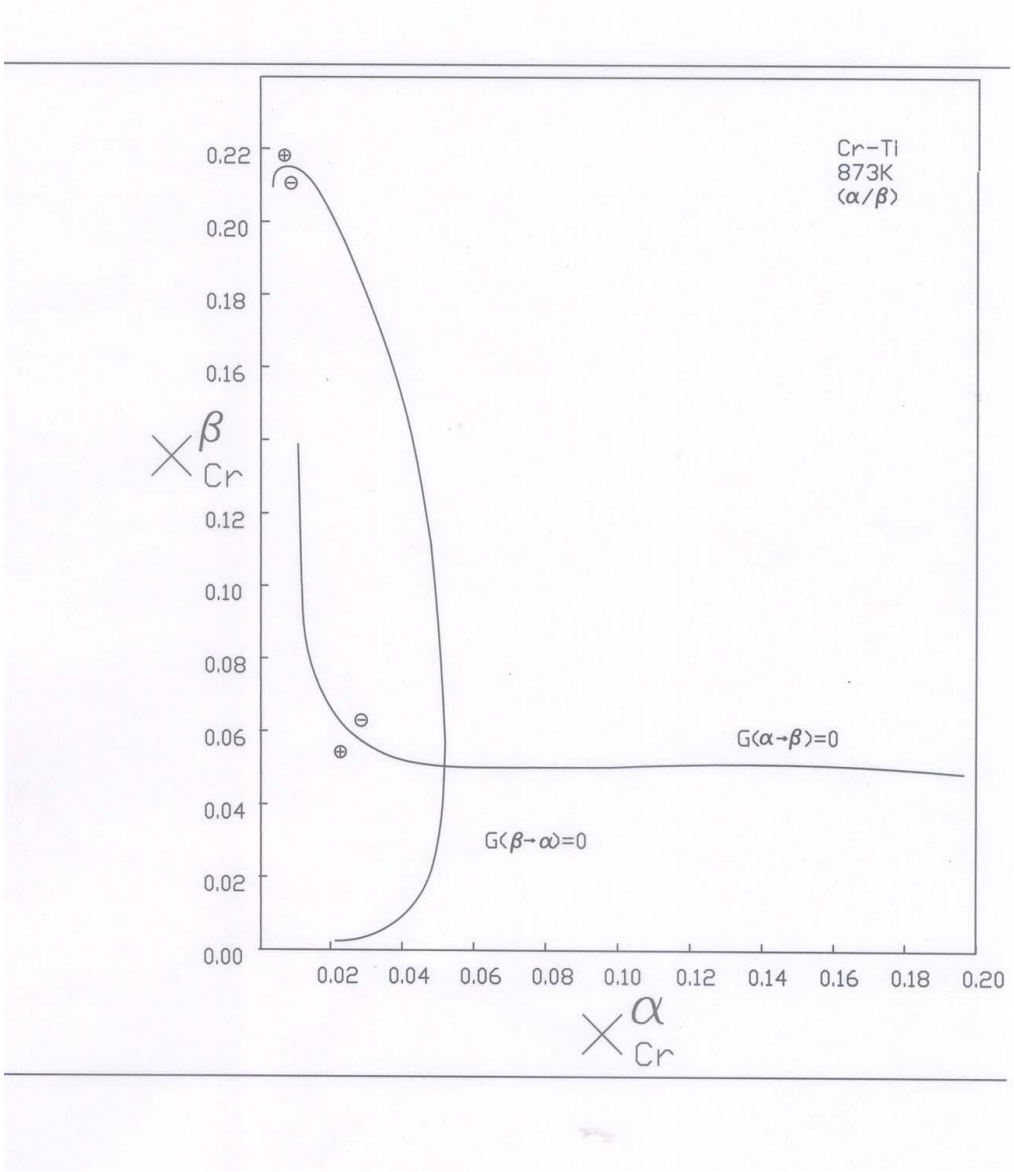

Fig. 6.4 The α/β Region of the Transformation Diagram of the Cr-Ti System at 873 K

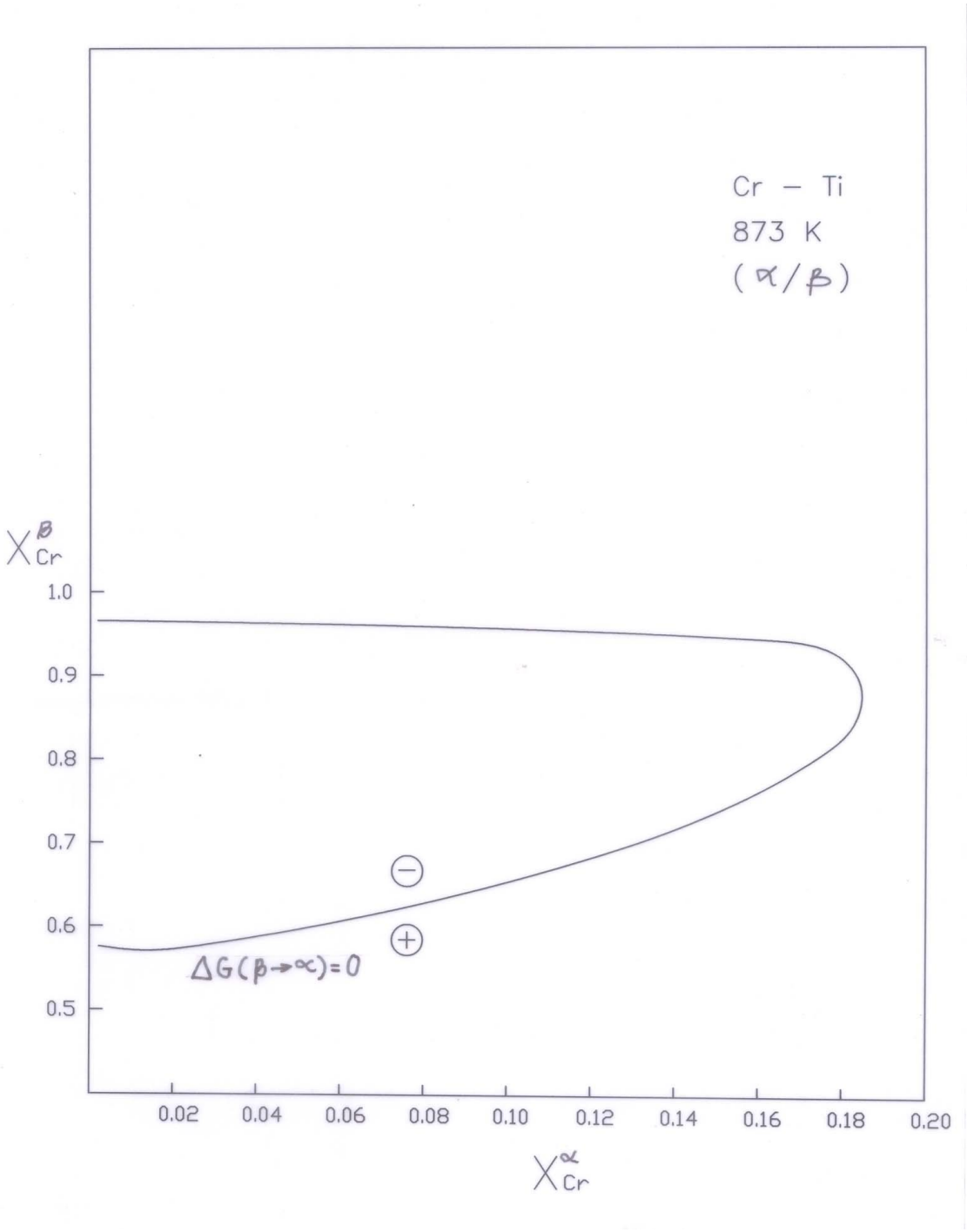

Fig. 6.5 The α/β Region of the Transformation Diagram of the Cr-Ti System at 873 K (at higher Cr levels in the β Phase)

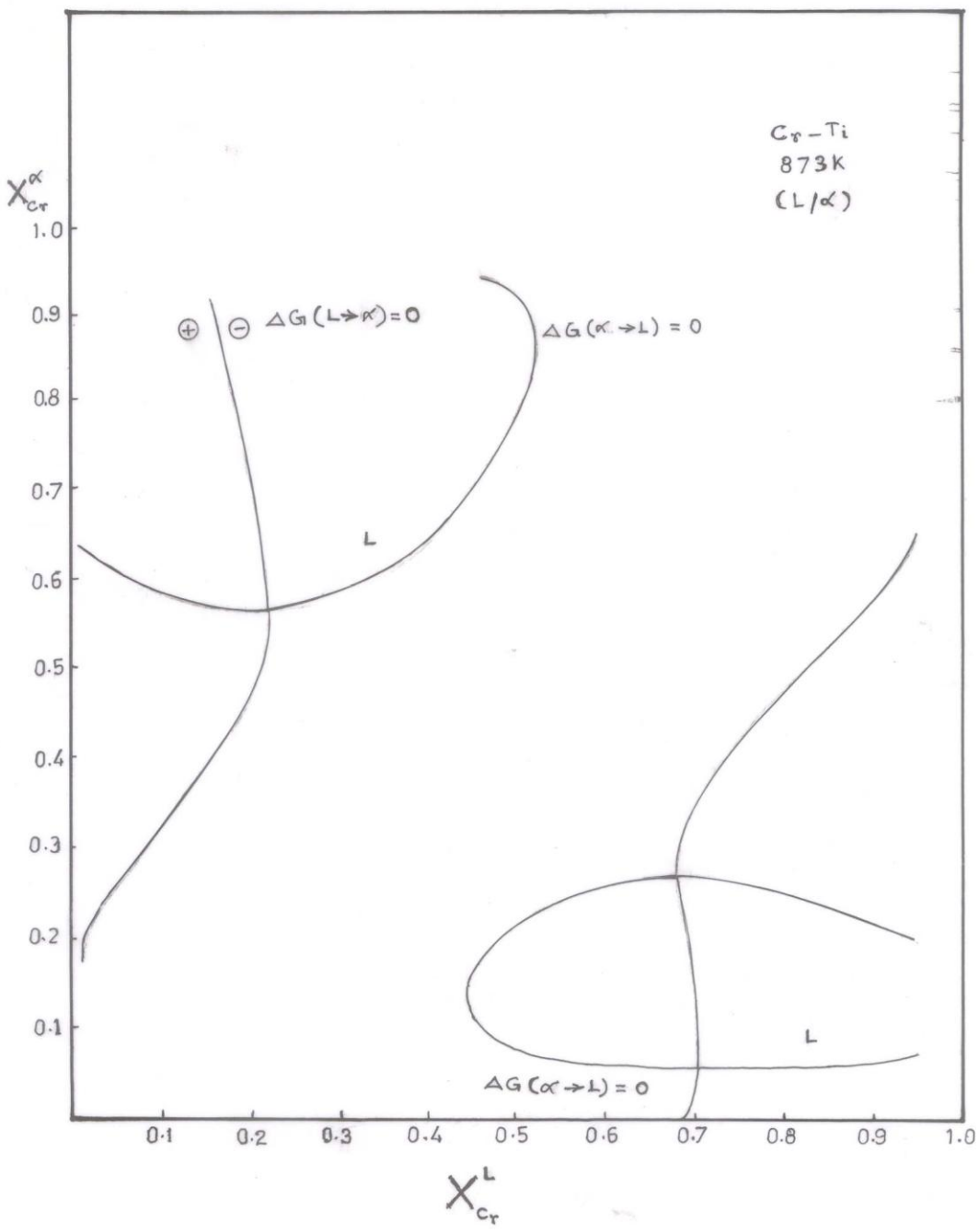

Fig. 6.6 The L/α Region of the transformation Diagram in the Cr-Ti System at 873 K

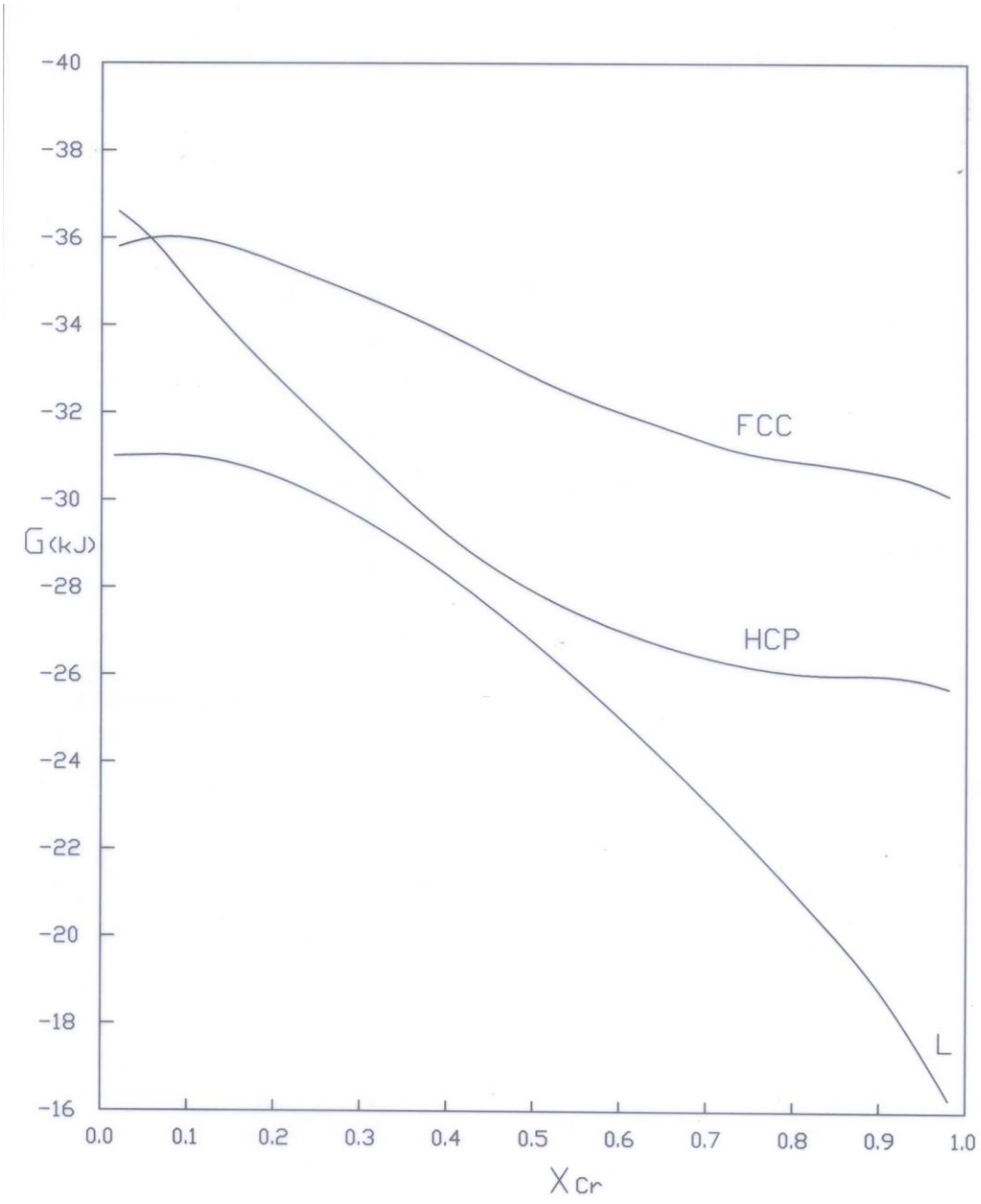

Fig. 6.7 The free Energy-Composition Diagram in the Cr-Ti System at 873 K

7. Construction of Transformation Diagrams – The Software Package

A software was developed for rapid computation and display of Transformation Diagrams of titanium-binary systems. The code was developed using Visual Basic language. It requires 256 RAM and can be run on any standard personal computer meeting these requirements of memory as has MS Office 2003.

The first screen of the package is depicted in fig. 7.1. the user selects the binary system of choice among the Ti-Cr, Ti-Cu, Ti-Mn and Ti-Nb systems. The second screen in fig. 7.2 allows the user to select the pair of phases from among liquid-bcc; hcp-bcc and liquid-bcc. The option on intermetallic compound and the corresponding range of activities are not active in the screen, at present. The user enters the desired temperature at which the Transformation Diagram has to be developed, in the window at the bottom. When the 'compute' button is pressed, the 'GSM' and the 'GLM' values required for constructing the Transformation Diagrams are displayed as shown in fig. 7.3. 'GSM' gives the range o composition over which transformation from Phase 1 to Phase 2 is feasible thermodynamically. 'GLM' gives the range over which transformation from Phase 2 to phase 1 is feasible. Phase 1 and Phase 2 represent the first and the second phase given in the listing on the left. The user presses the "refresher" button on this screen to reach the next screen, shown in fig. 7.4. On reaching this screen, the "Insert" button on the task bar is activated. Inside this pull down menu, the "chart" option is chosen (fig. 7.5). In the "chart wizard", "XY(scatter)" option is chosen (fig. 7.6). This displays the Transformation Diagram as illustrated in fig. 7.7, for a specific case, that of liquid-bcc transformation in the Ti-Cr system at 873 K. Figures 7.8, 7.9 and 7.10 give the hcp-bcc (at 873 K); liquid-hcp (at 873 K)and liquid-bcc (at 1773 K) Transformation Diagrams in the Ti-Cr system, respectively. Figure 7.11 to 7.19 give the Transformation Diagrams in eth Ti-Cu and Ti-Mn systems. The system chosen, the temperature and the pairs of phases selected are indicate don each diagram.

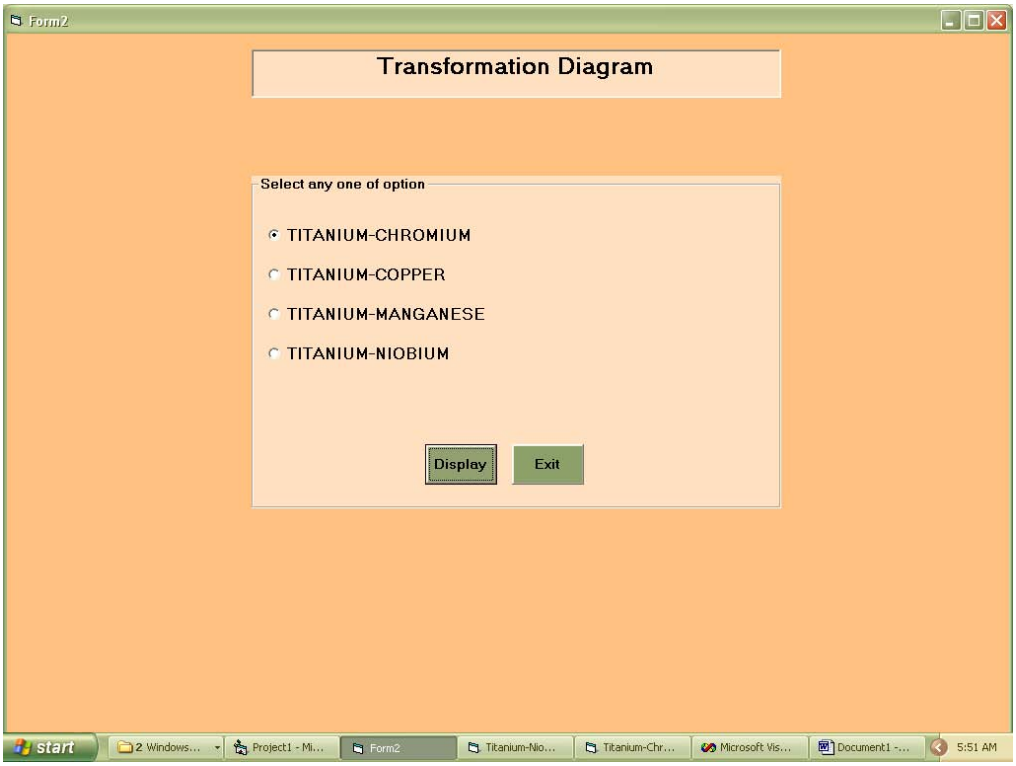

Fig.1 Transformation Diagram – Screen 1

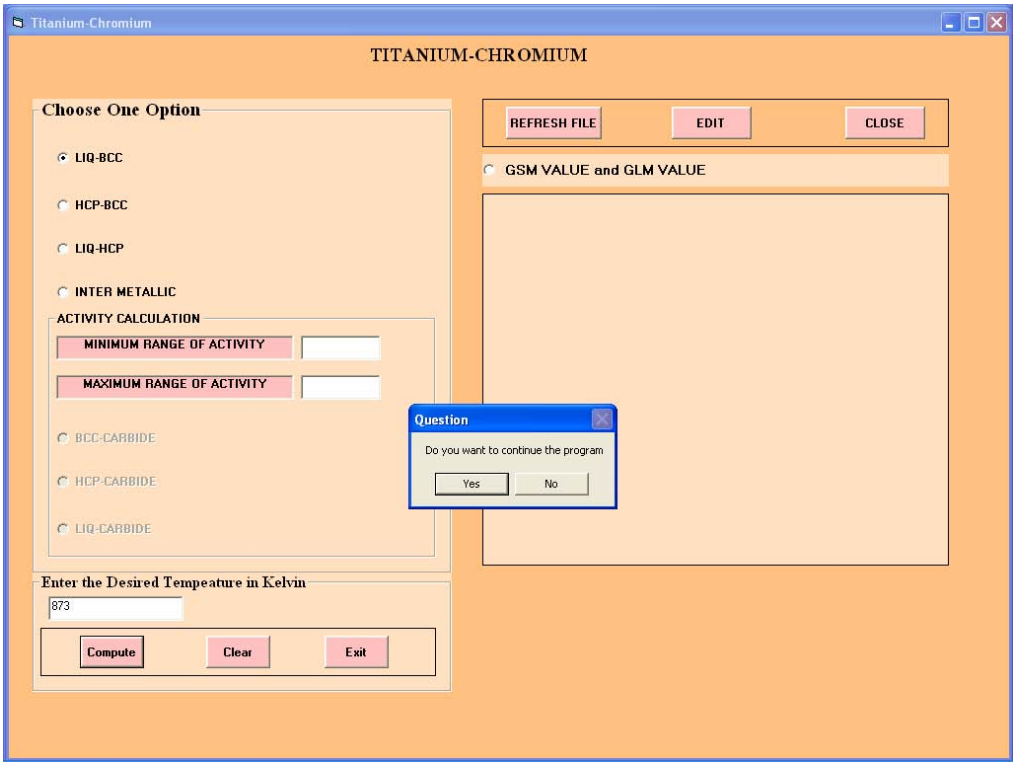

Fig.2 Transformation Diagram – Ti-Cr-Screen 2

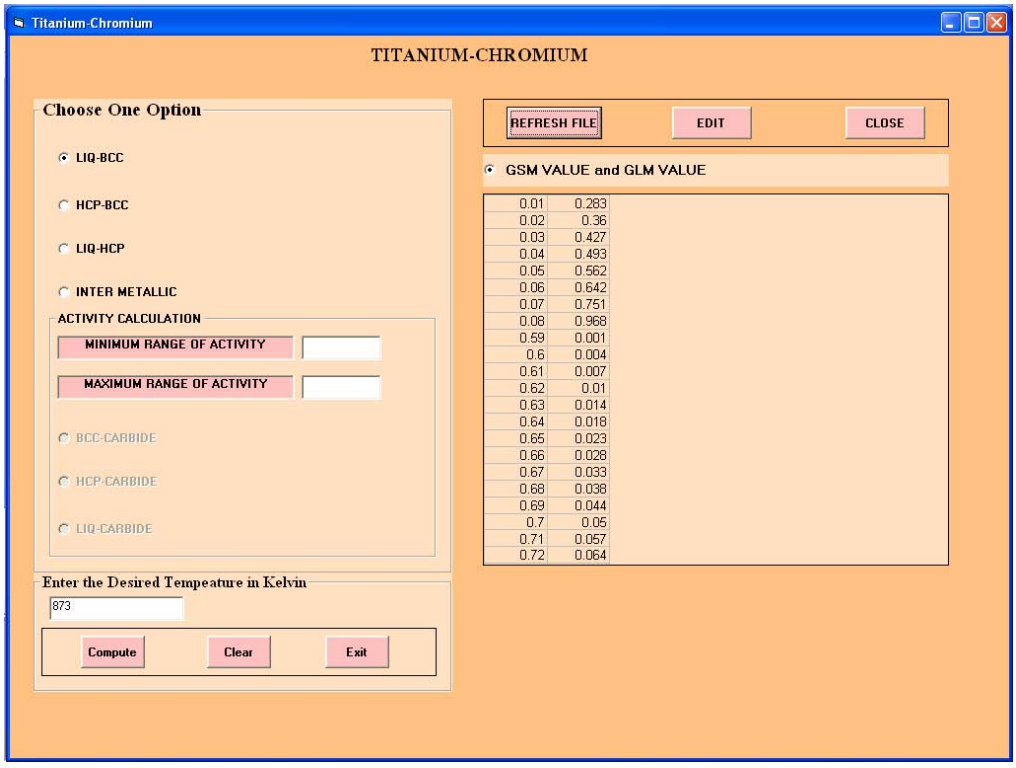

Fig.3 Transformation Diagram – Ti-Cr-Screen 3

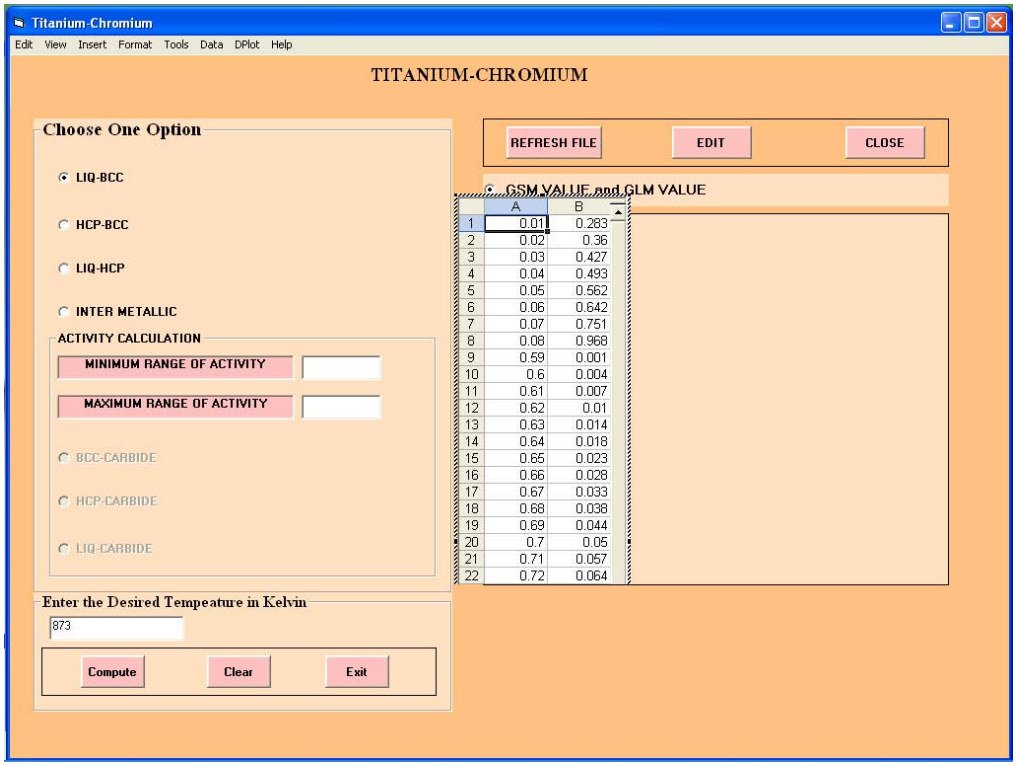

Fig.4 Transformation Diagram – Ti-Cr-Screen 4

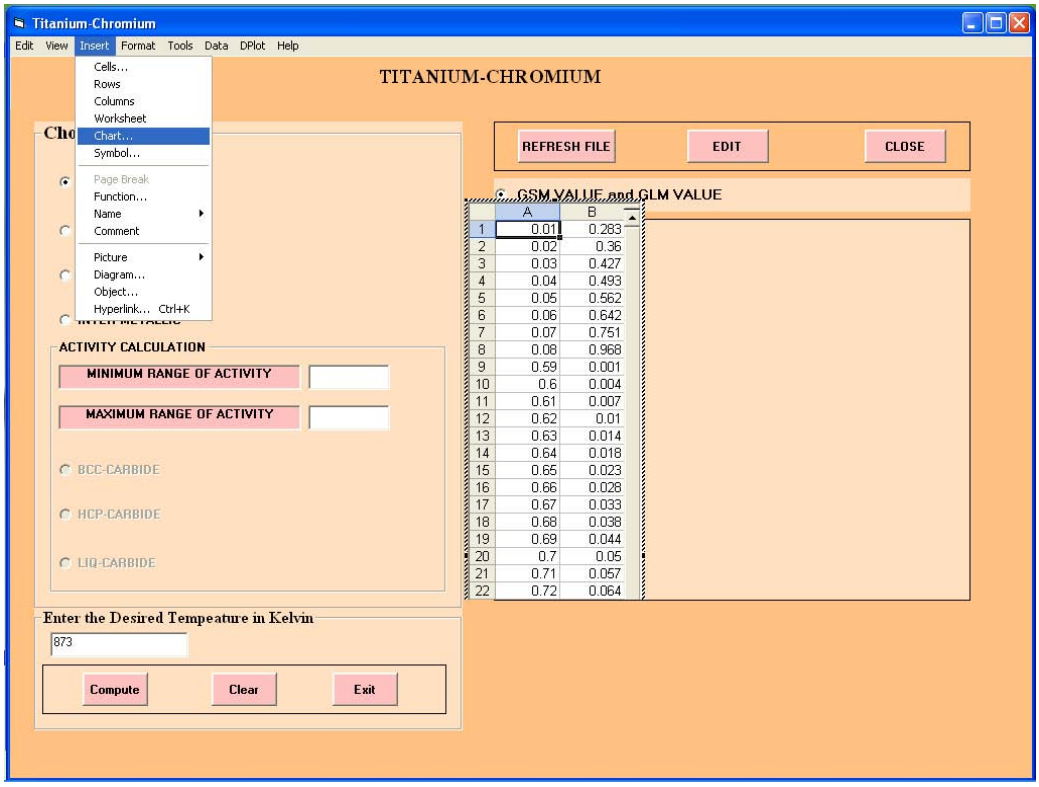

Fig.5 Transformation Diagram – Ti-Cr-Screen 5

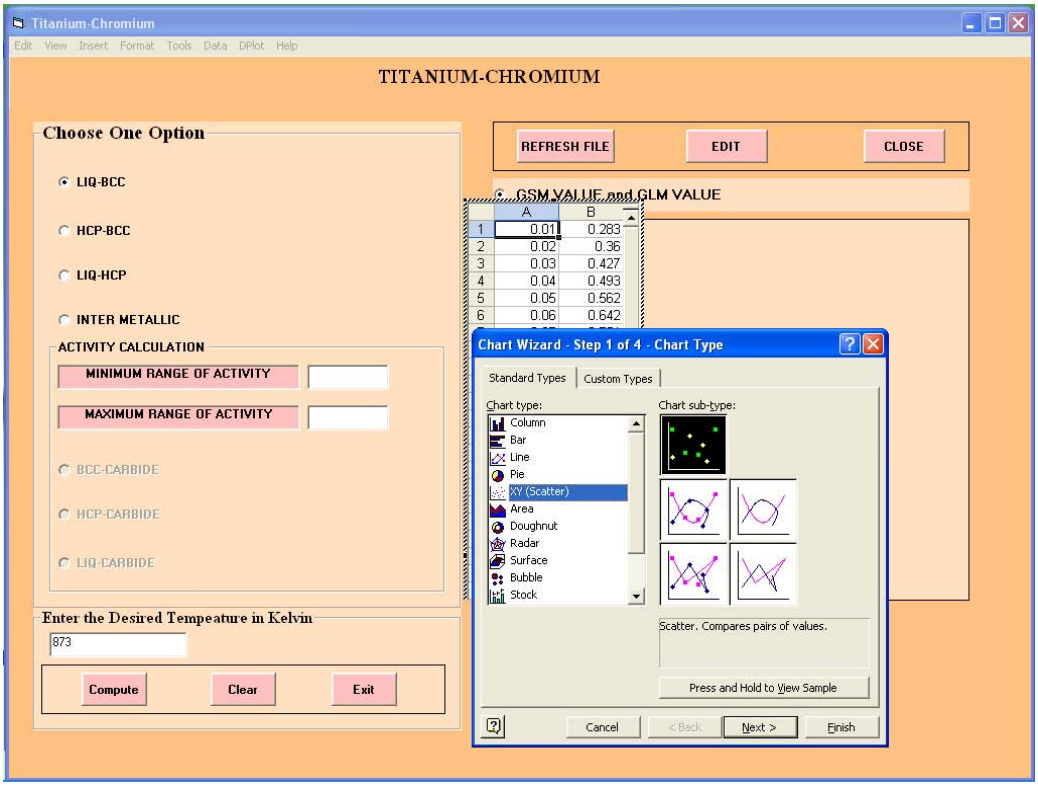

Fig. 6 Transformation Diagram – Ti-Cr-Screen 6

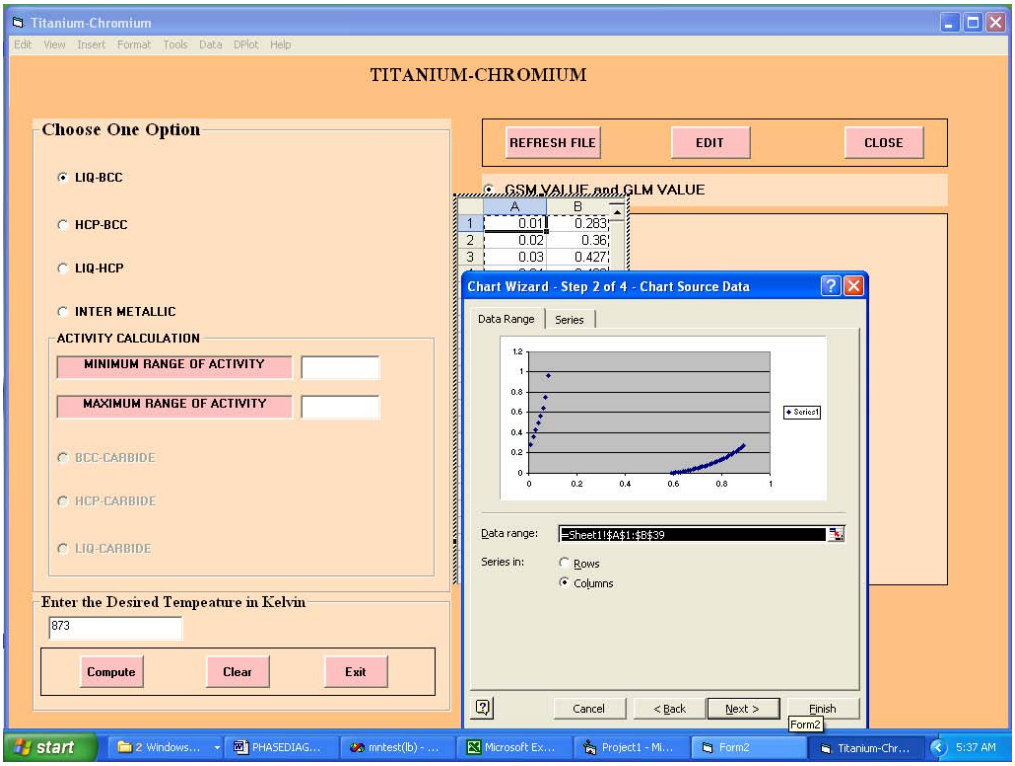

Fig. 7 Transformation Diagram – Ti-Cr-Screen 7

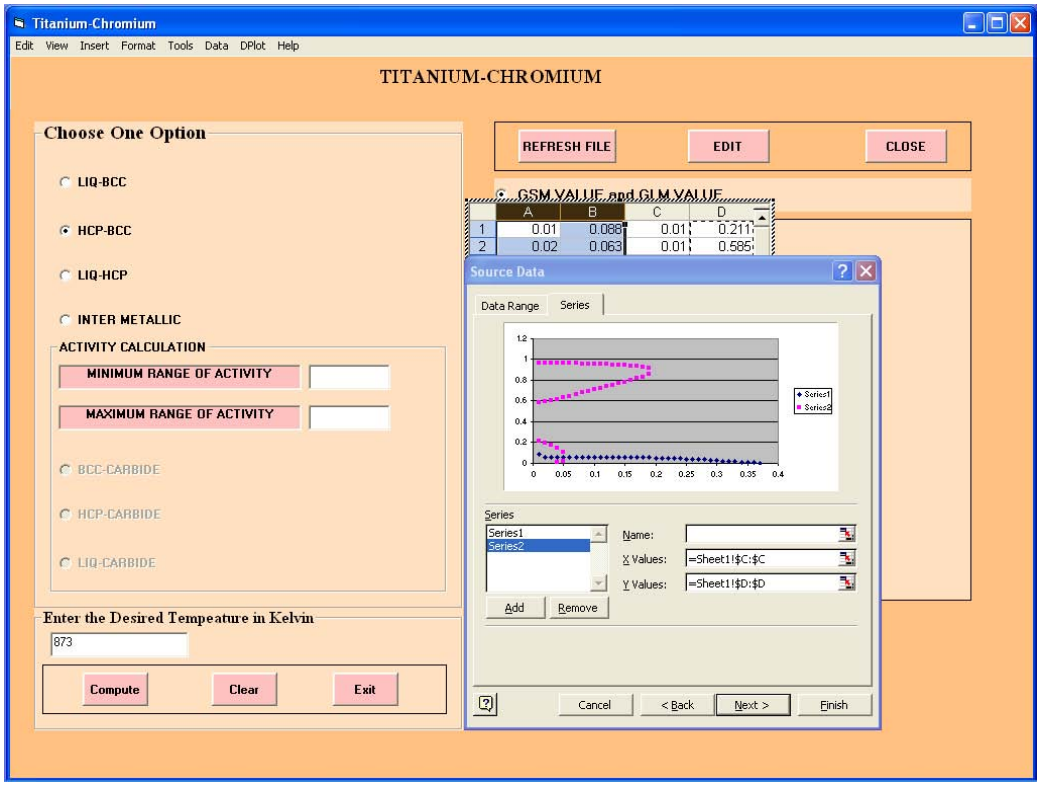

Fig.8 Transformation Diagram – Ti-Cr-Screen 8

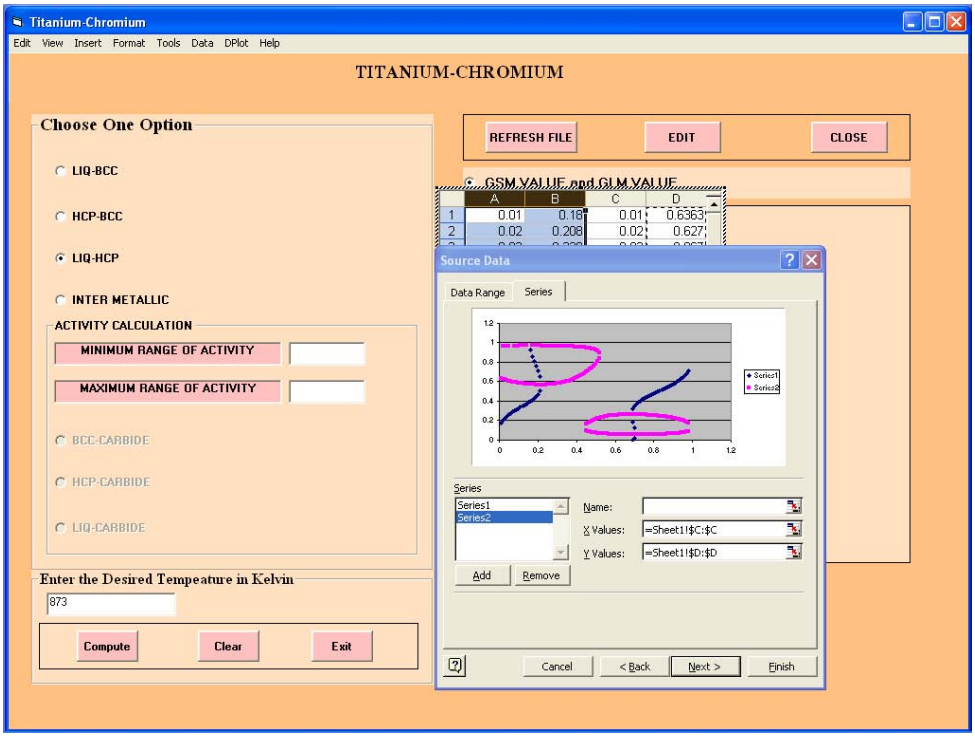

Fig. 9 Transformation Diagram – Ti-Cr-Screen 9

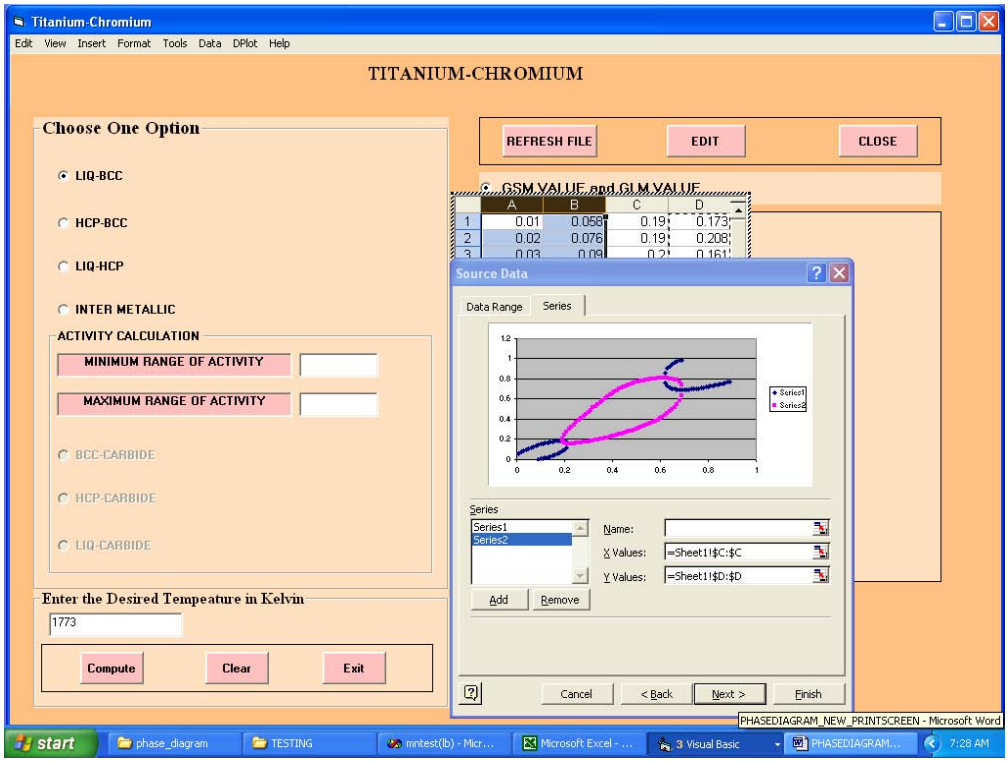

Fig.7.10 Transformation Diagram – Ti-Cr-Screen 10

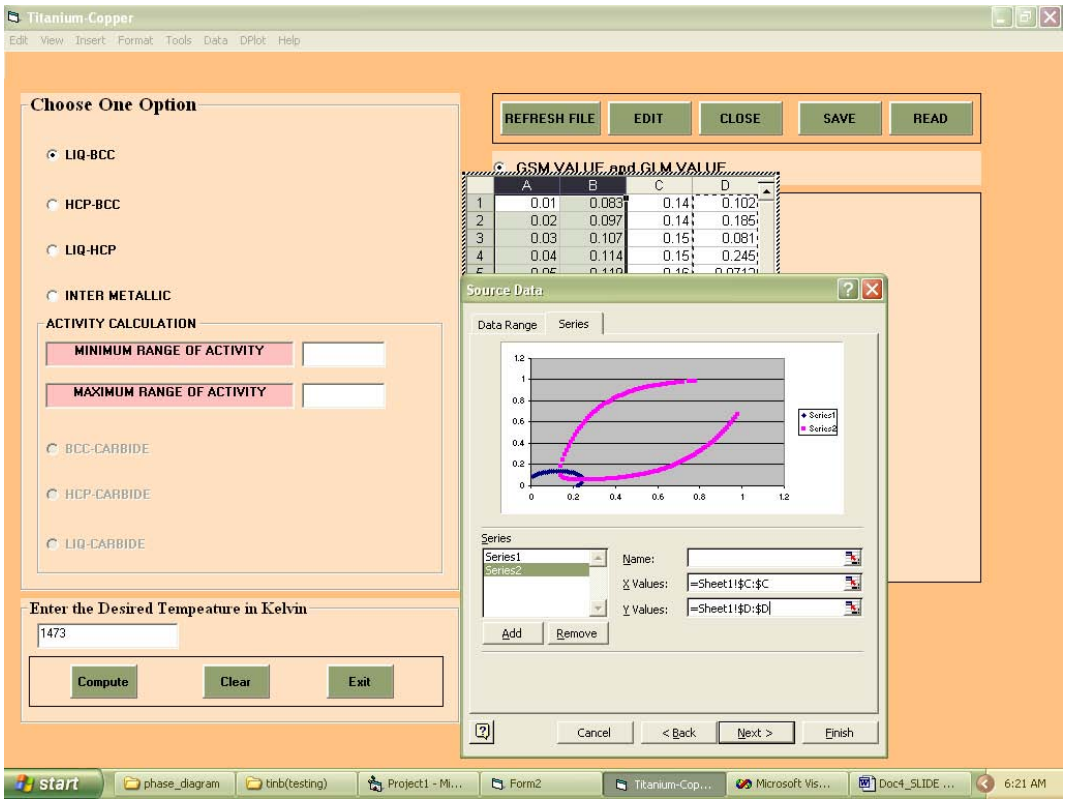

Fig.7.11 Transformation Diagram – Ti-Cu-Screen 11

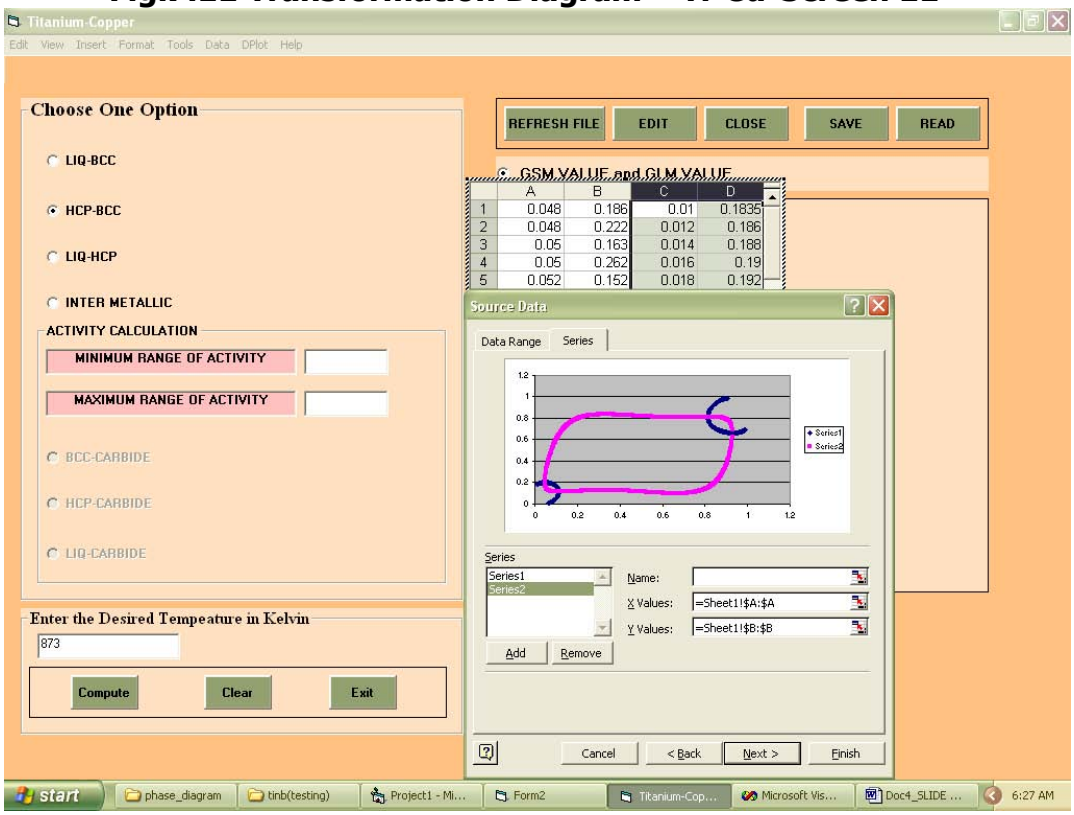

Fig.7.12 Transformation Diagram – Ti-Cu-Screen 12

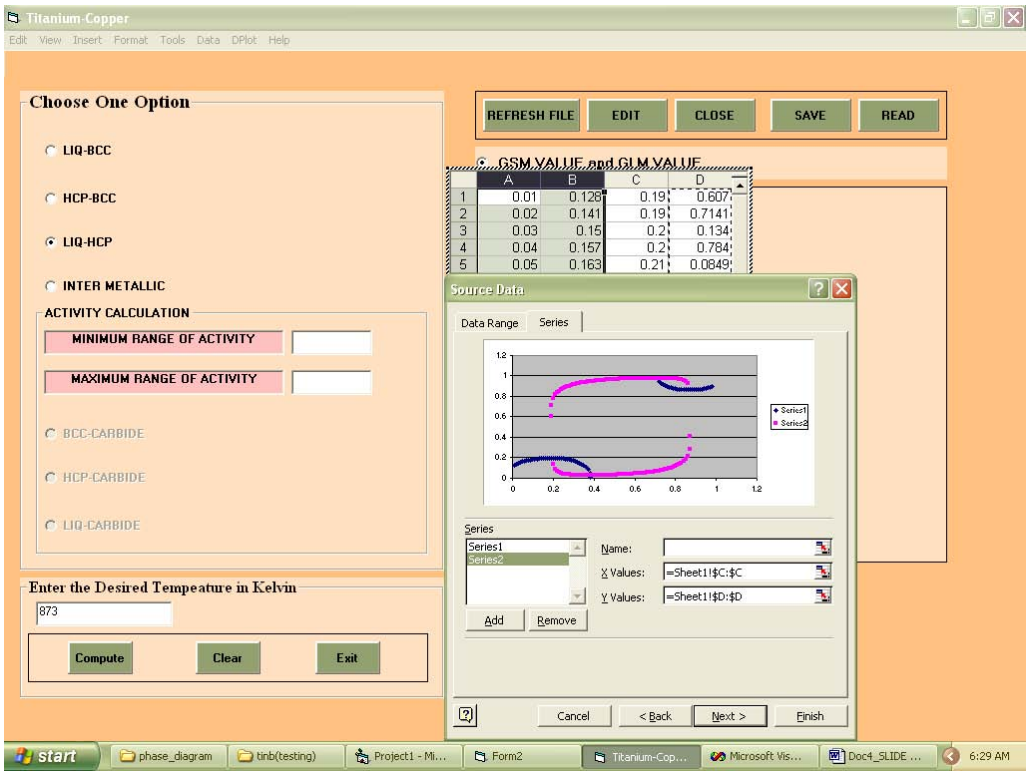

Fig.7.13 Transformation Diagram – Ti-Cu-Screen 13

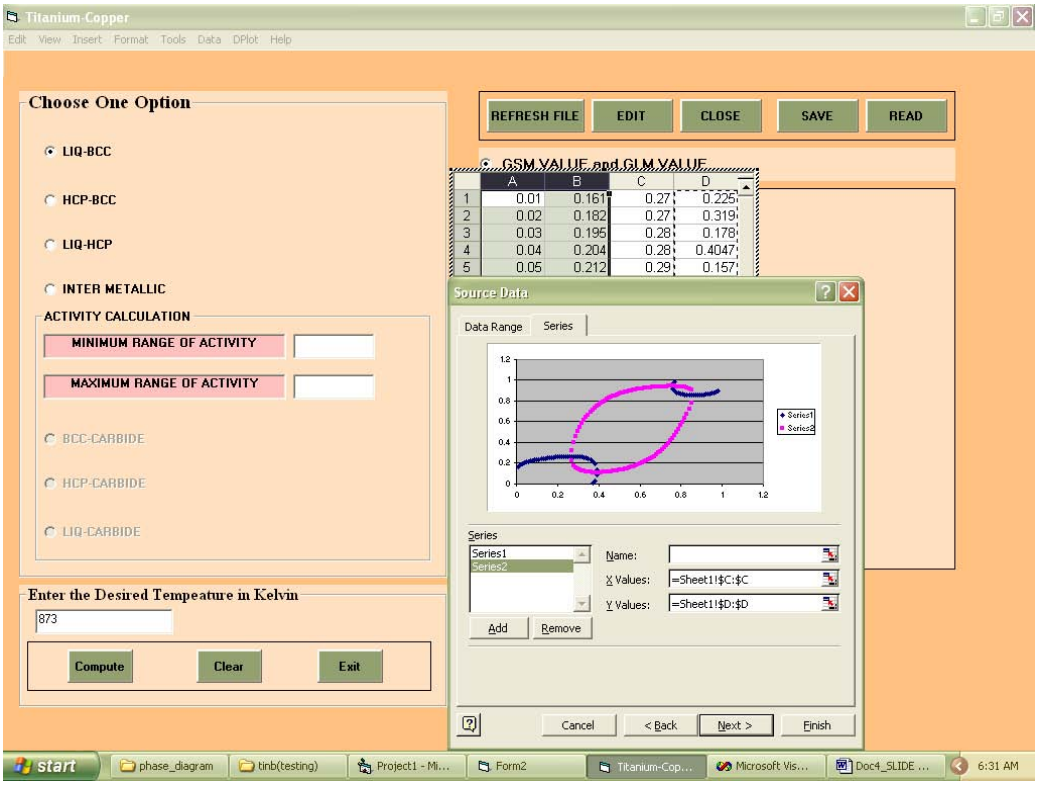

Fig.7.14 Transformation Diagram – Ti-Cu-Screen 14

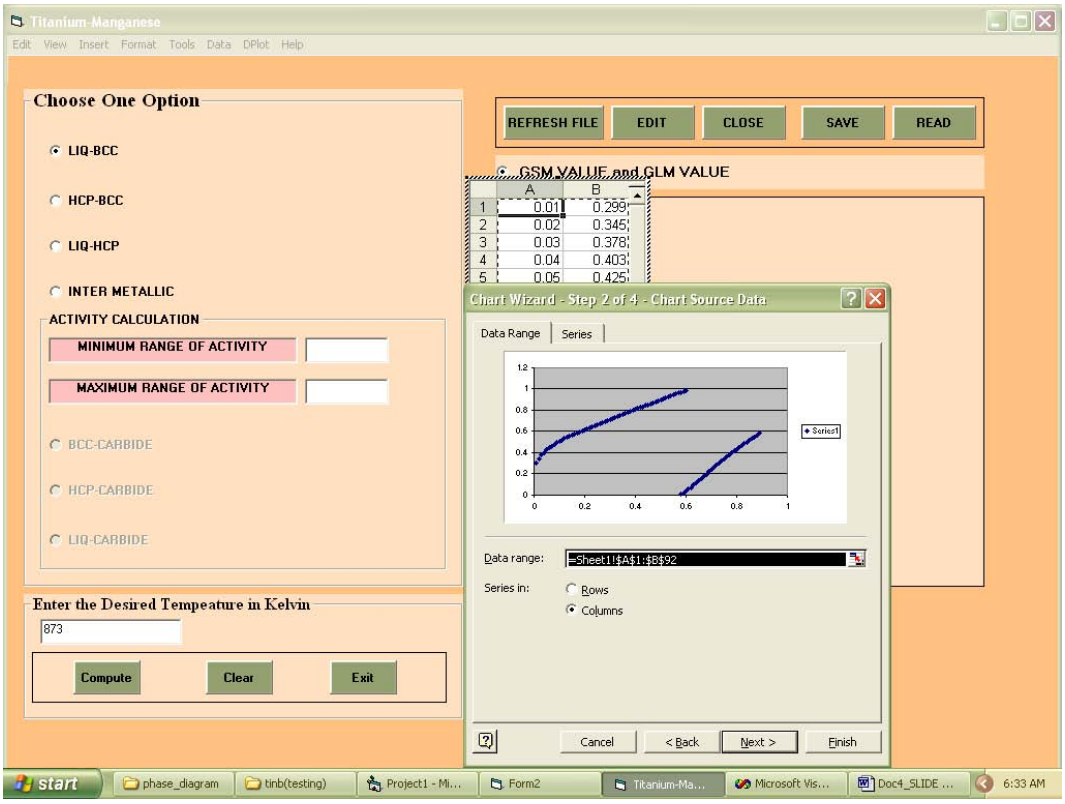

Fig.7.15 Transformation Diagram – Ti-Mn-Screen 15

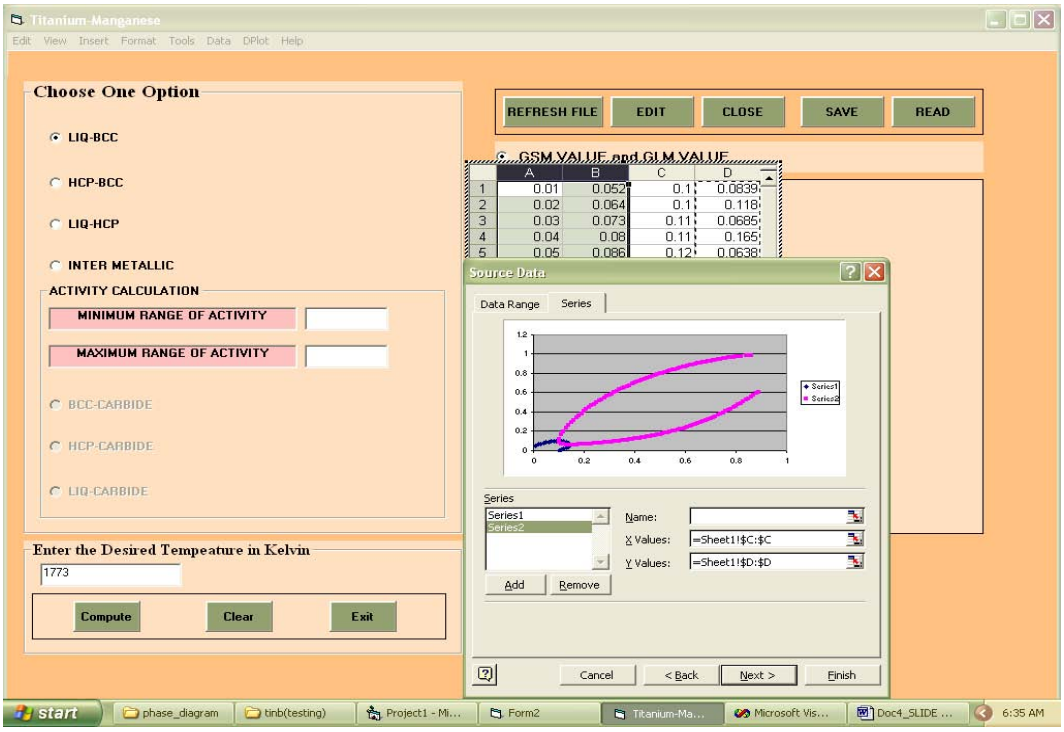

Fig. 7.16 Transformation Diagram – Ti-Mn-Screen 16

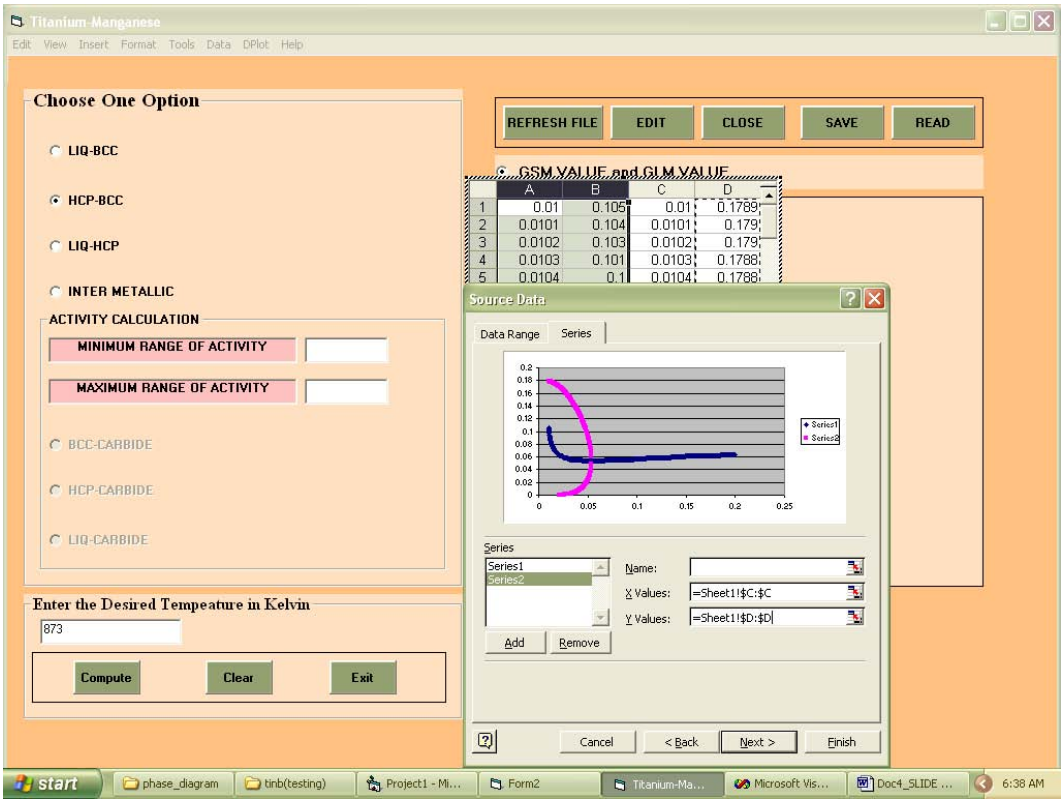

Fig.7.17 Transformation Diagram – Ti-Mn-Screen 17

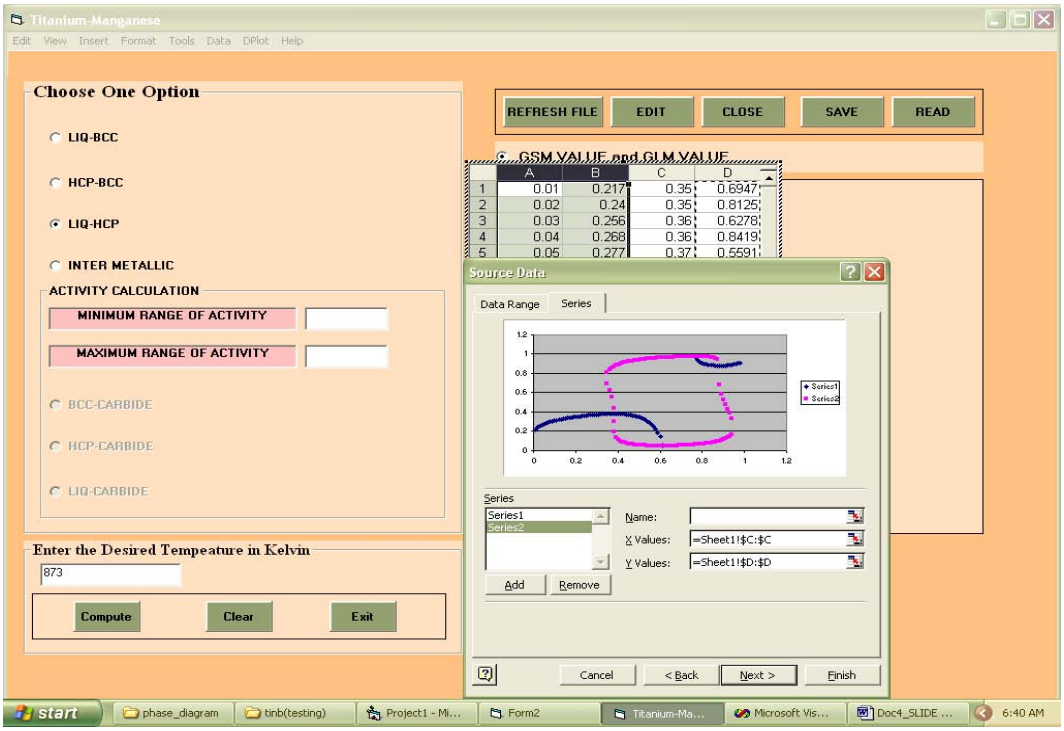

Fig.7.18 Transformation Diagram – Ti-Mn-Screen 18

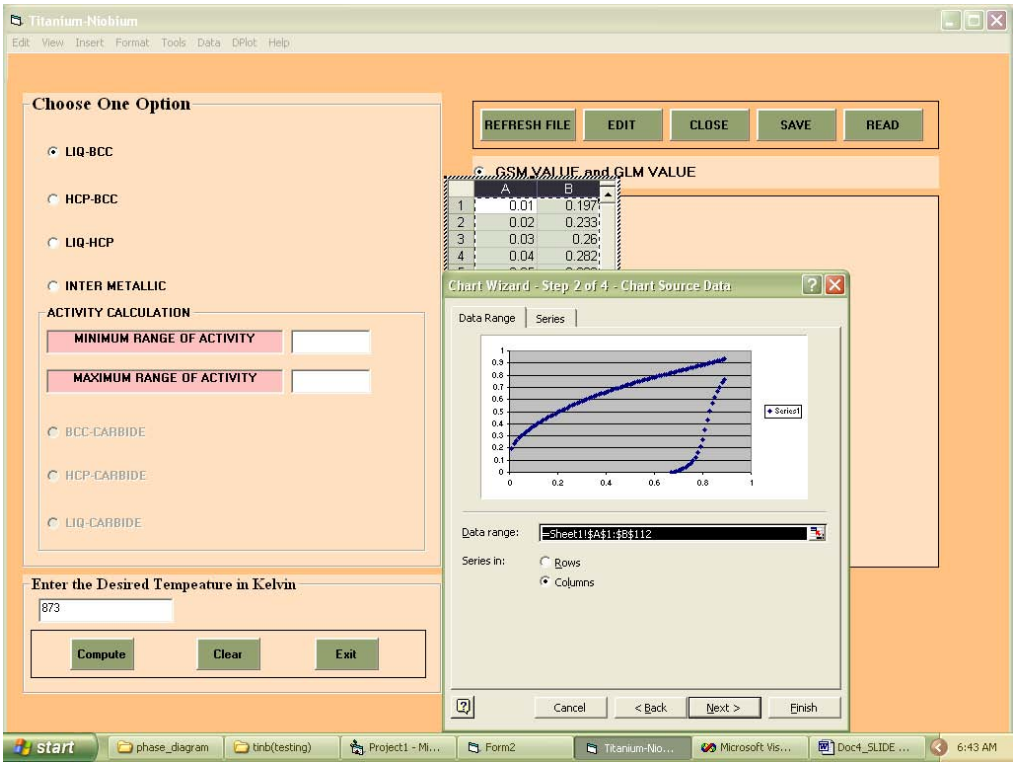

Fig. 7.19 Transformation Diagram – Ti-Cr-Screen 19

8. Experiments on Spontaneous Vitrification

Experiments were carried out to study the process of spontaneous vitrification in titanium-binary alloys. Titanium rods, 99.99% purity; chromium prices, 99.99% purity; and copper shots, 99.99% purity were used in the preparation of the binary alloys. Titanium pieces and the desired binary component were melted in arc under argon atmosphere, to prepare the binary alloys. They were cast in water cooled-copper moulds in the form of buttons 20 mm diameter, 10 mm thick. Hemispheres of alloy 10 mm thick, 20 mm diameter were cut out from the buttons and used in the experiments.

The alloy disc was placed in a quartz capsule about 15 mm diameter, 50 mm length. The capsule was evacuated, refilled with argon and evacuated again. This process was repeated three times before, the capsule was sealed under vacuum. The sealed capsule was placed inside a tubular furnace for annealing at the desired temperature. Each capsule was first annealed at 1200 °C for four hours in the case of the Ti-Cr alloys. It was then quenched in water and the alloy disc was recovered. The recovered disc was again encapsulate din a quartz capsule following the same procedure as described above. The second capsule was held at 600 °C inside the tubular furnace for a desired period of time. At the end of this period, the capsule was quenched in water and the alloy disc recovered. A few discs were cut from the original alloy equilibrated at 1200 °C. Each of the discs was held at 600 °C for different periods of time. At the end of this period, the disc was subjected to XRD analysis to identify the phases present.

Fig. 8.1 gives the XRD pattern of Ti-Cr alloy (X_{Cr}=0.72) after equilibration at 1200 °C. The peaks are sharp and the presence of bcc-Cr and $TiCr_2$ phases could be confirmed. These phases are expected to be present at equilibrium at 1200 °C for this composition.

Fig. 8.2 gives the XRD of the alloy above held at 600 °C for 48 hours after initial equilibration at 1200 °C. The peaks are still sharp and there is no evidence of amorphisation. Bcc-Cr and $TiCr_2$ phases ere identified in the alloy.

Fig. 8.3 is the XRD of the same alloy examined in fig. 8.1 but held for 8 days at 600 °C after quenching from 1200 °C. Many of the peaks seen in fig. 8.1 and fig. 8.2 have disappeared and there is considerable broadening of the residual peaks indicating that amorphisation has already occurred. Bcc-Cr and Cr_2Ti were the crystalline phases identified in this sample.

Fig. 8.4 is the XRD of a second composition of Ti-Cr alloy (X_{Cr}=0.4) after equilibrtation at 1200 °C. Fig. 8.5 is the XRD of this sample after a holding time of 8 days at 600 °C. Fig. 8.5 contains no sharp peak. This indicates that amorphisation has occurred in this case also. Bcc-Cr and hcp-Ti phases were present in this alloy.

Fig. 8.6 gives the XRD of a Ti-Cu alloy (X_{Cu}=0.2) held at 600 °C for 8 days after initial equilibration at 1200 °C. there is evidence of vitrification indicated by the broadening of peaks and the absence of sharp peaks. HCP-Ti and and Ti_2Cu phases were identified in this alloy.

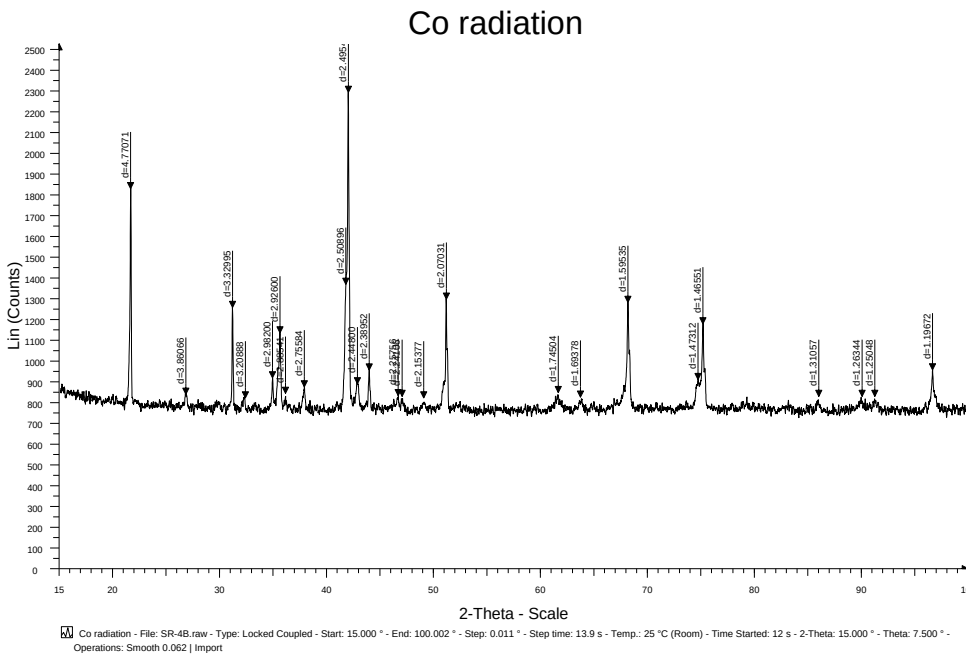

Fig. 8.1 Ti-Cr Alloy-1 Equilibrated at 1200 °C

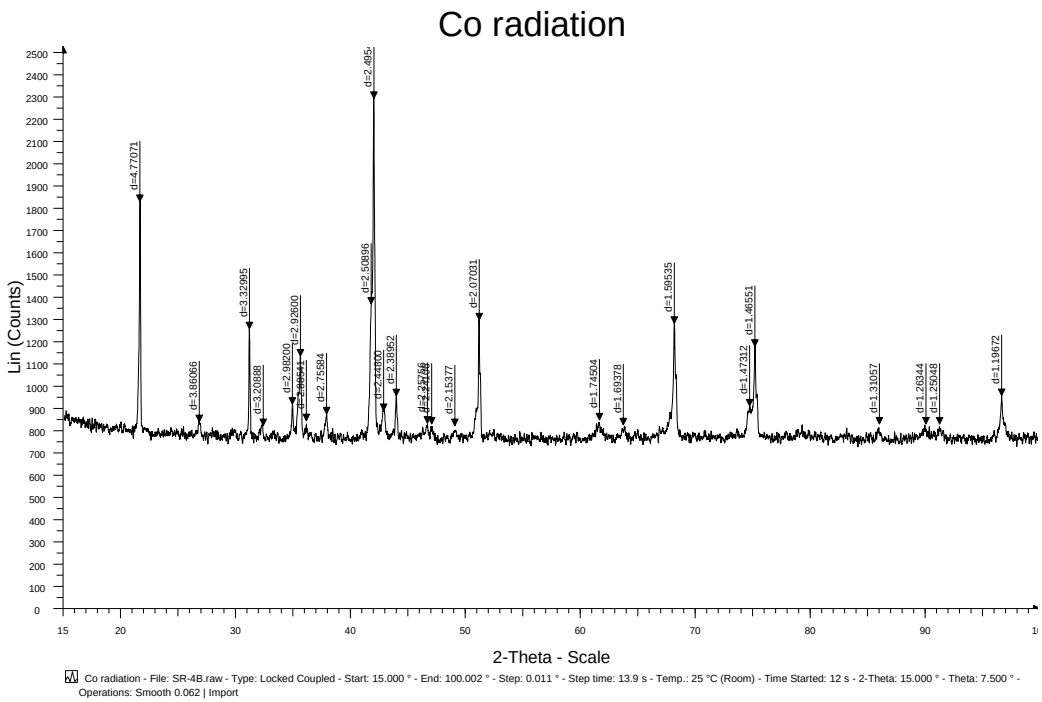

Fig. 8.2 Ti-Cr alloy-1 Annealed at 600 °C, 48 hrs

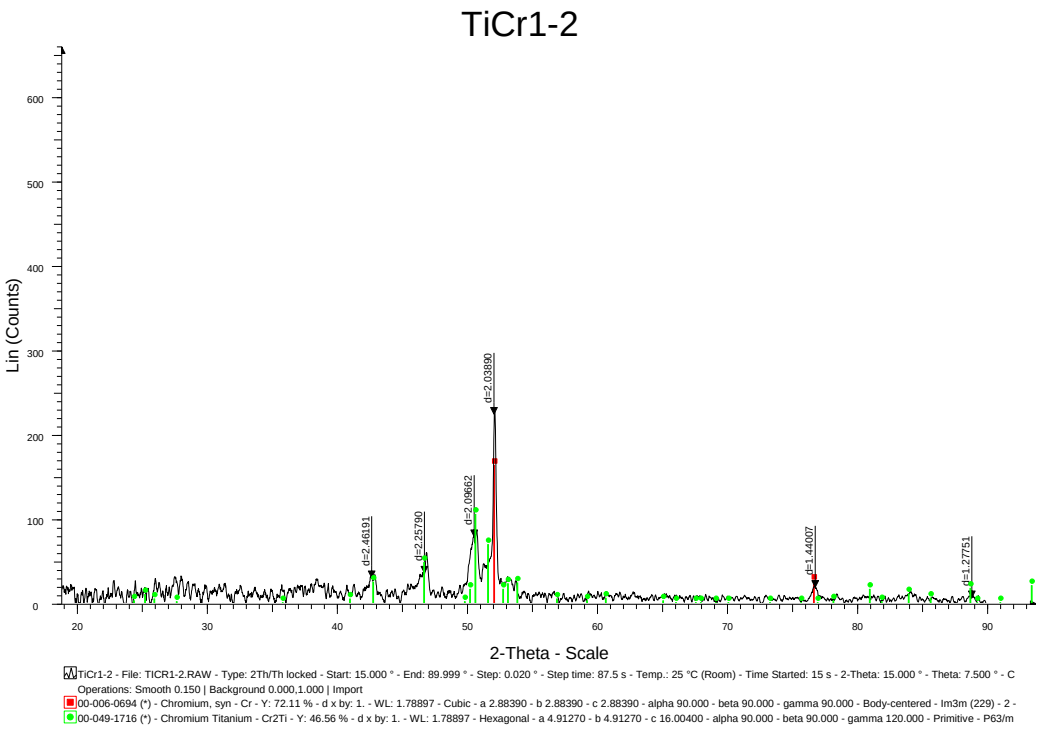

Fig. 8.3 Ti-Cr Alloy-1, Annealed at 600 C, 8 days

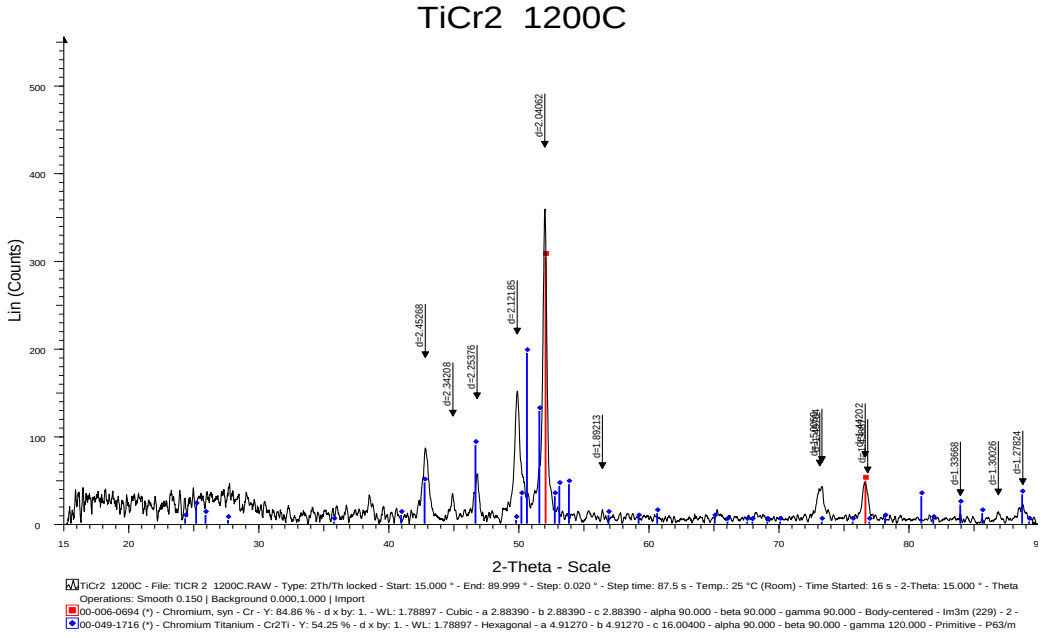

Fig. 8.4 Ti-Cr Alloy-2, Equilibrated at 1200 °C

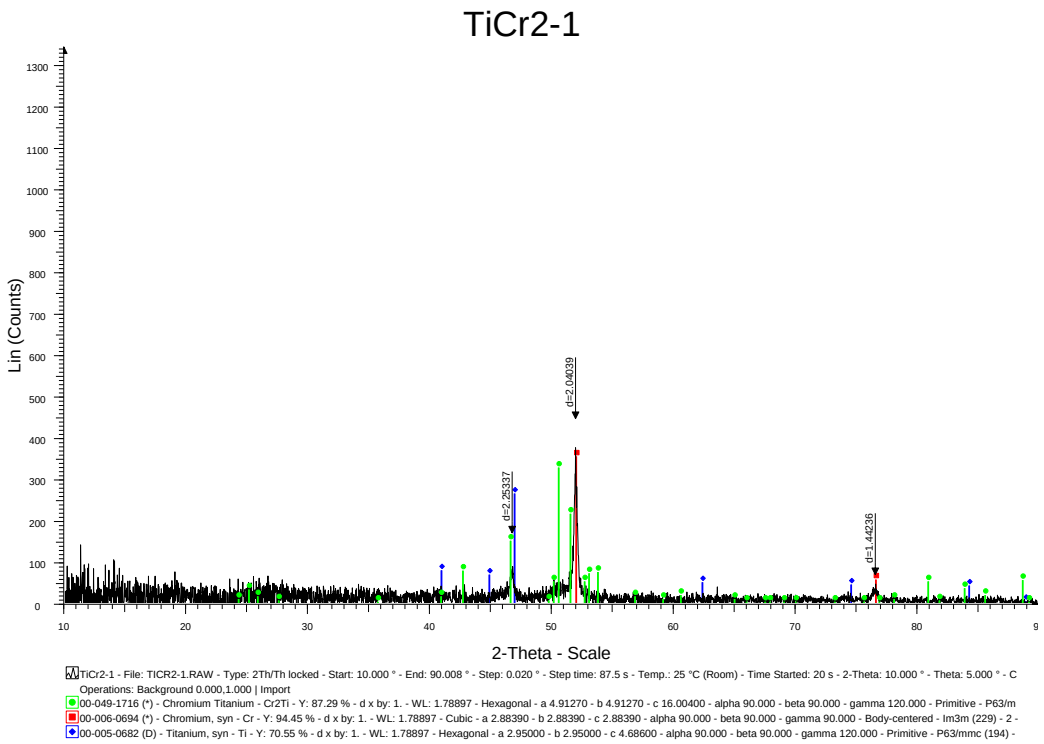

Fig. 8.5 Ti-Cr Alloy-2, Annealed at 600 °C, 8 days

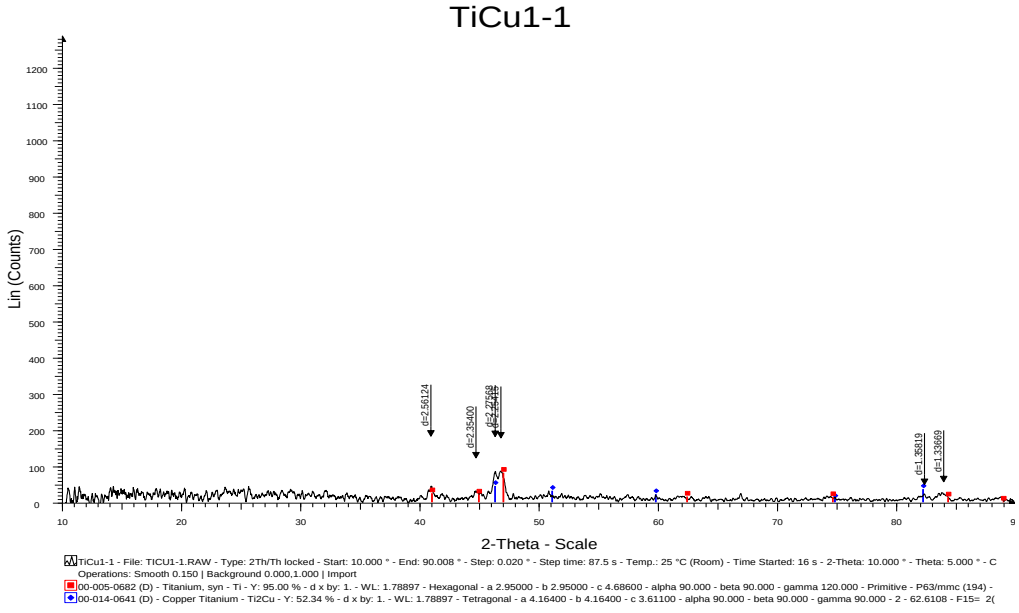

Fig. 8.6 Ti-Cu Alloy, Annealed at 600 °C, 8 days

9. Validation and Discussion

9.1 Validation

Extensive experimental study has been reported in literature on spontaneous vitrification in Ti-Cr system. Thermodynamic models have been constructed to rationalize the observations. The salient experimental observations in this system have been :

(a) Polymorphous transformation between bcc and amorphous phase occurs in the Ti-Cr system at X_{Cr}=0.3 and at X_{Cr}=0.55.

(b) At a few other compositions, residual β phase has been observed along with the amorphous phase.

(c) The ω phase has been observed to be formed during spontaneous vitrification.

(d) Splat-cooled samples do not show spontaneous vitrification on annealing at low temperatures.

The thermodynamic models discussed in literature have assumed an equilibrium-type transformation between the two meta-stable phases, viz. the quenched bcc and the amorphous phase. Meta-stable equilibrium diagrams have been constructed based on this approach. The accuracy of the thermodynamic data used in the modeling is low and the "phase boundaries" predicted by these phase diagrams are unreliable. These issues have been already highlighted in previous chapters. These models can not explain the presence of the ωphase along with the amorphous phase. These models forbid polymorphous transformation at X_{Cr}=0.3, but observed in experiments. These are serious limitations of the thermodynamic models presented in literature.

The Transformation Diagrams can consistently rationalize the experimental observations. In the chapter on "Transformation diagrams for Ti-binary Systems", it was demonstrated that the bcc phase can not transform to the amorphous at 873 K, since it is not feasible thermodynamically. On the other hand, the bcc phase can transform to the hcp phase at this temperature. Reference to fig. 6.5 shows informs that the bcc phase of composition X_{Cr}=0.6 can transform to the hcp phase of composition of about

X_{Cr}=0.06. Reference to fig. 6.6 shows that the hcp phase of composition X_{Cr}=0.06 would transform to the amorphous phase of composition X_{Cr}=0.6 and above. Therefore, an alloy of composition X_{Cr}=0.6 would appear to undergo a polymorphous transformation under certain circumstances. The composition of the product phase would depend on the diffusivity of atoms, the holding time etc.

Fig. 9.1 is the Transformation Diagram for hcp-bcc transformation in the Ti-Cr system at 773 K. This shows that an alloy of composition X_{Cr}=0.3 in the bcc phase can transform to a hcp phase of composition X_{Cr}=0.5. Fig. 9.2 gives the Transformation Diagram for the hcp-liquid transformation at the same temperature in this system. This figure shows that the alloy of composition X_{Cr}=0.05 can transform from the hcp phase to an alloy of composition X_{Cr}=0.7 in the amorphous phase. Therefore, the net transformation is that of an alloy of composition X_{Cr}=0.3 transforming from the bcc phase to the amorphous phase. It is interesting to note that a polymorphous transformation has been observed at this composition from bcc to amorphous phase(1) in this system. The conventional thermodynamic models have rejected this observation as *impossible*(11). The Transformation Diagrams show that this polymorphous transformation is possible. This agreement with experimental observation is another major success of the Transformation Diagrams compared to the conventional thermodynamic analysis.

The discussions above show that the meta-stable phase transformations occur through significant fluctuations in composition although over very short distances. These fluctuation have to take place in opposite directions for the transformation to be complete. Presence of defects such as vacancies crated during quenching assist in the rearrangement of atoms by providing adequate vacant space for this process to occur. Splat-cooled samples contain very low concentrations of defects. Hence, these samples do not show the *bcc→amorphous* transformation which actually proceeds through the formation of the hcp phase as an intermediate.

9.2 Conclusion

Transformation Diagrams have been constructed for titanium-binary systems such as Ti-Cr, Ti-Cu and Ti-Mn. A software package has been developed for rapid construction of these diagrams. The predictions of the Transformation diagrams have been validated using experimental data available in literature. These Diagrams are successful in explaining several phenomena observed experimentally during spontaneous vitrification in Ti-binary alloys but could not be explained using conventional thermodynamic modeling of the transformation process. Experiments were conducted to study the phenomenon of spontaneous vitrifitaion in Ti-Cr and Ti-Cu alloys. These studies confirm the predictions of the Transformation Diagrams.

9.3 Acknowledgement

Financial assistance received from the Asian Office of Aerospace Research and Development under contract No. AOARD-07-4038, for carrying out this research work is gratefully acknowledged.

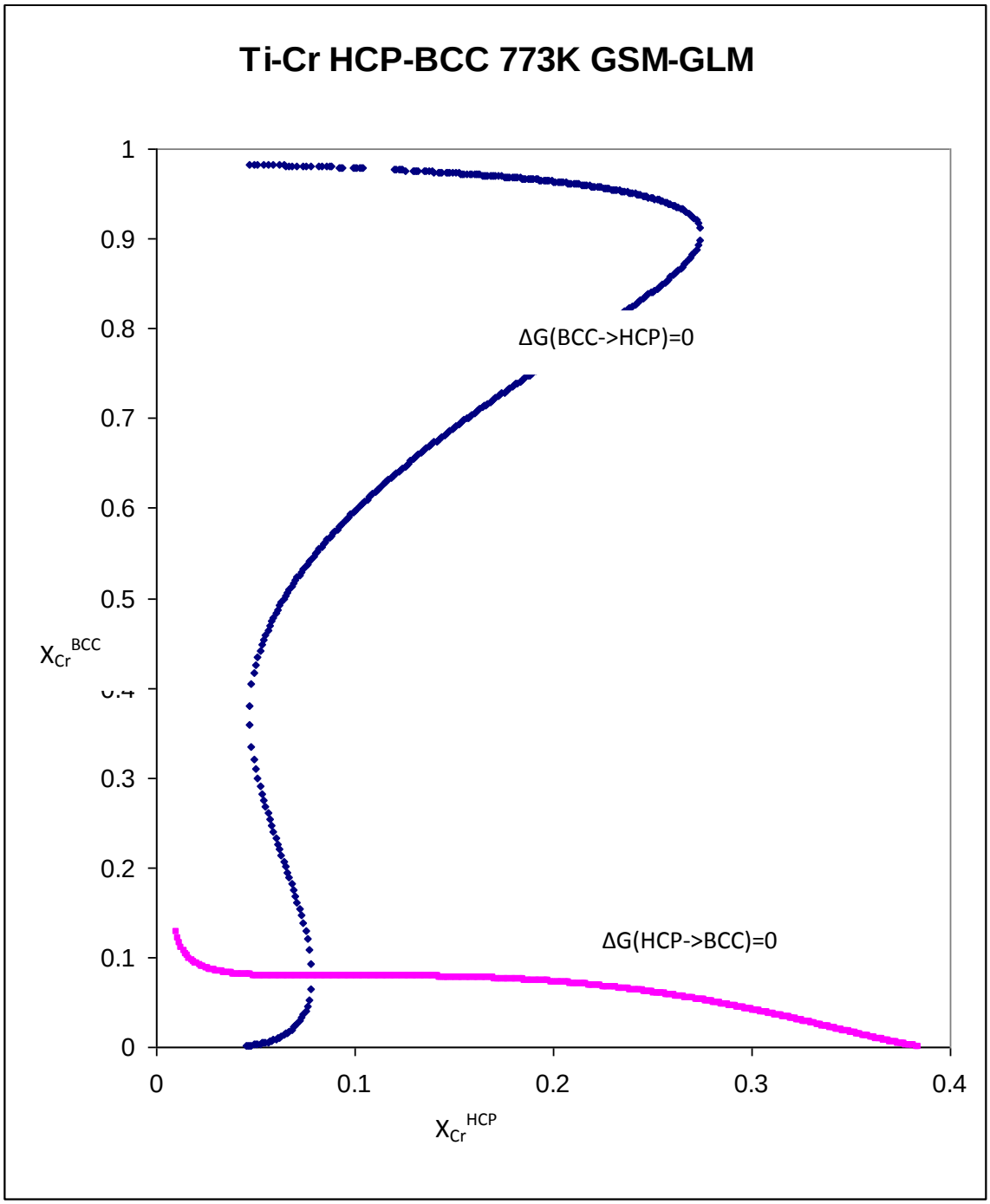

Fig. 9.1 Transformation Diagram Ti-Cr, 773 K, HCP-BCC

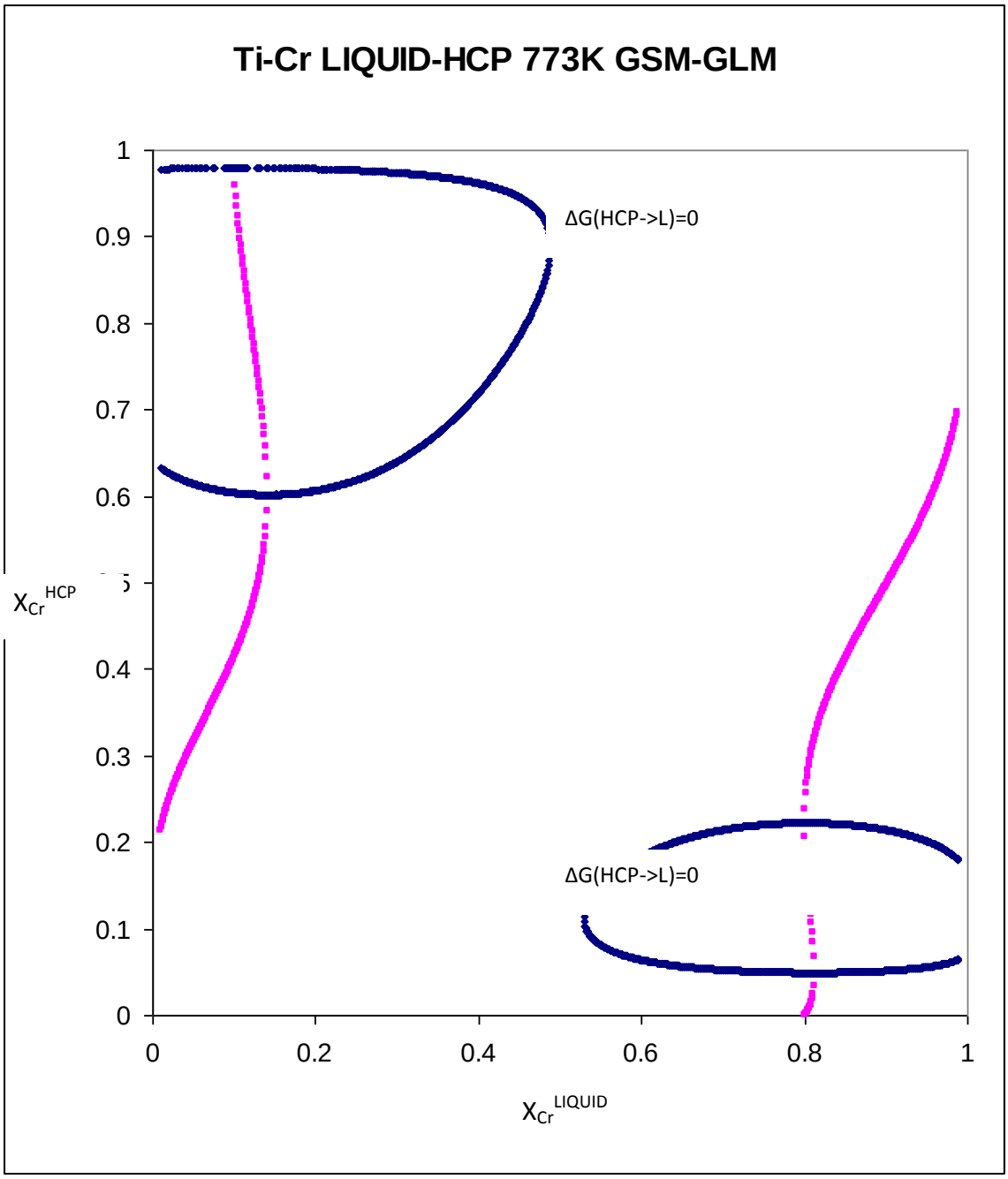

Fig. 9.2 Transformation Diagram Ti-Cr, 773 K, HCP-LIQUID

10. Bibliography

1. A. Blatter and M. von Allmen, Reversible Amorphisation in Laser-Quenched Titanium Alloys, Physical review Letters, 13 May 1985, **54**(19), 2103-2106.
2. M. von Allmen and A. Blatter, Spontaneously Vitrifying Crystalline Alloys, Appl. Phys. Lett., **50**(26), 29 June 1987, 1873-1875.
3. A. Blatter, J.Gfeller and M.von Allmen, Structure and Transfomation Kinetics in Spontaneously Vitrified Cr-Ti Alloys, J. Less Common Metals, **140**(1988), 317-325.
4. A. Blatter,U.Kambli, Ch.Wirz, R.Giovanoli, K.Drybye and J.Bottiger, Role of Defects in the Spontaneous Vitrification of β-(Cr,Ti), Phys. Review B, **40**(18), 15 Dec. 1989, 12503-12507.
5. A. Silberstein, P.C.Clapp and L.E.Tanner, J. Less-Common Metals, **140**(1988), 245-
6. H.Hsieh and S.Yip, Phys. Rev. Lett. **59**(1987), 2760-
7. L.J. Gallego, J.A. Samoza and J.A. Alonso, Possibility of Spontaneous Vitrification in Ti-Cr Alloys, Physica B, **160** (1989), 108-112.
8. Yong-Gyoo Kim and Jai-Young Lee, A Kinetic Study on the Spontaneous Vitrification of Cr40Ti60 Alloy, J. of Non-Crystalline Solids, **122**(1990) 269-275.
9. Ch. Wirz and A. Blatter, Transformation Preceding Amorphisation in Cr-Ti and Cr-Ti-Fe β phases, Physical Review B, **42**(11), 15`Oct. 1990, 6993-7001.
10. K.Ohsaka, E.H.Trinh, J.C.Holzer and W.L. Johnson, Gibbs Free Energy Difference Between the Undercooled Liquid and the β Phase of a Cr-Ti Alloy.
11. Z.H. Yan, T.Klassen, C.Michaelsen, M.Oehring and R.Bormann "Inverse Melting in the Cr-Ti System", Physical Review B, 1 April 1993, **47**(14), 8520-8529.
12. R.Bormann, Thermodynamic and Kinetic Requirements for Inverse Melting, Mater. Sci. and Engg., A179/A180(1994), 31-35.
13. A.Blatter, M.von Allmen and N.Baltzer, J.Appl. Phys., **62**(1), 1 July 1987, 276-

280.

14. A.L. Greer, the thermodynamics of Inverse melting, J. Less Common Metals, **140**, 327-334, June 1988.
15. Baker J.C. and Cahn J.W., 1970, *Solidification,* Am. Soc. Metals, Metals Park, Ohio, 23-58.
16. Markus Rettenmayr, Oliver Warkentin and Hans Eckart Exner, Z.Metallkd., **88** (1997) 617-619.
17. M. Rettenmayr, 0. Warkentin, M. Rappaz and H.E. Exner, Acta mater. **49** (2001) 2499-2510.
18. Julius C.Schuster, Yong Du.. Calphad 1999; 23: 393
19. Duschanek H,, Rogl P, Lukas H.. J.Phase Equilibria 1995; 16:46
20. Dupin N, Ansara I. J.Phase Equilibria 1993; 14 : 451
21. M.Enomoto. J.Phase Equilibria 1992; 13:195
22. Banerjee R, Collins PC and Fraser HL. Metall. And Mater. Transactions 2002; 33A: 2129
23. Chandrasekaran V, Taggart R. Polonis DH. Metallography 1973; 6: 313
24. Ikematsu Y, Doi M, Miyazaki T. J. Mater. Sci.1991; 26 :2071
25. Mebed AM and Miyazaki T. Metall. And Mater. Transactions 1998; 29A **:**739
26. Narayanan GH, Archbold TF. Metall. Transactions 1970; 1 : 2281.
27. S.Ranganathan, P.Ramachanrarao. CALPHAD 2003; 27: 39
28. S.Ranganathan. Trans. Indian Inst. Met. 2002; 55 : 551
29. Binary Alloy Phase Diagrams, Vol. 1, Editor-in-chief, Thaddeus B. Massalski, American Society for Metals, Metals Park, Ohio 44073, 1986.

Appendix A

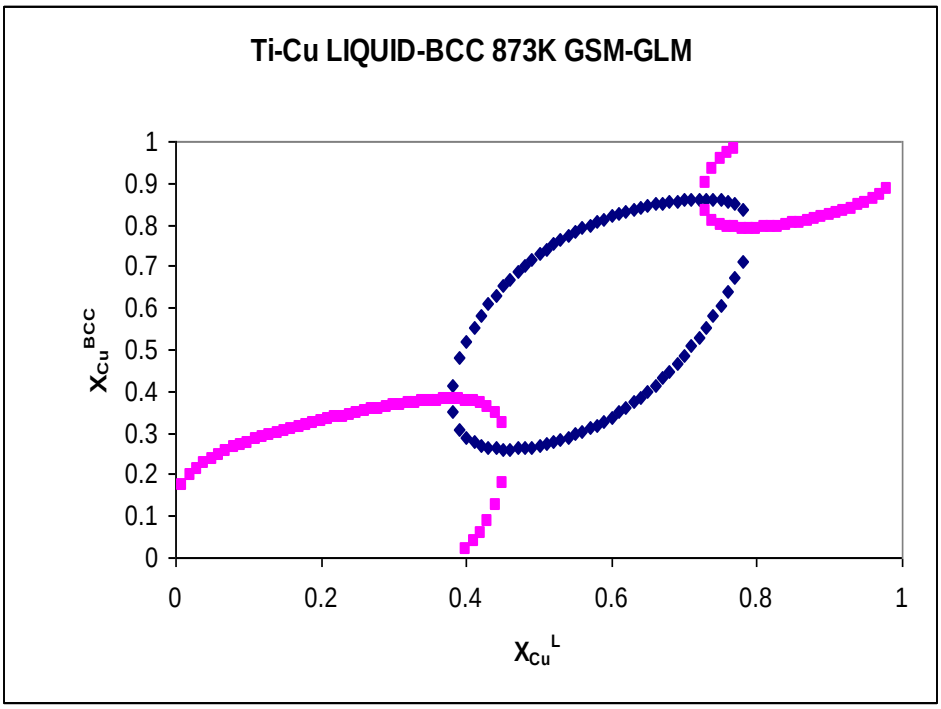

Fig. A.1 Transformation Diagram, Ti-Cu, Liquid-BCC, 873 K

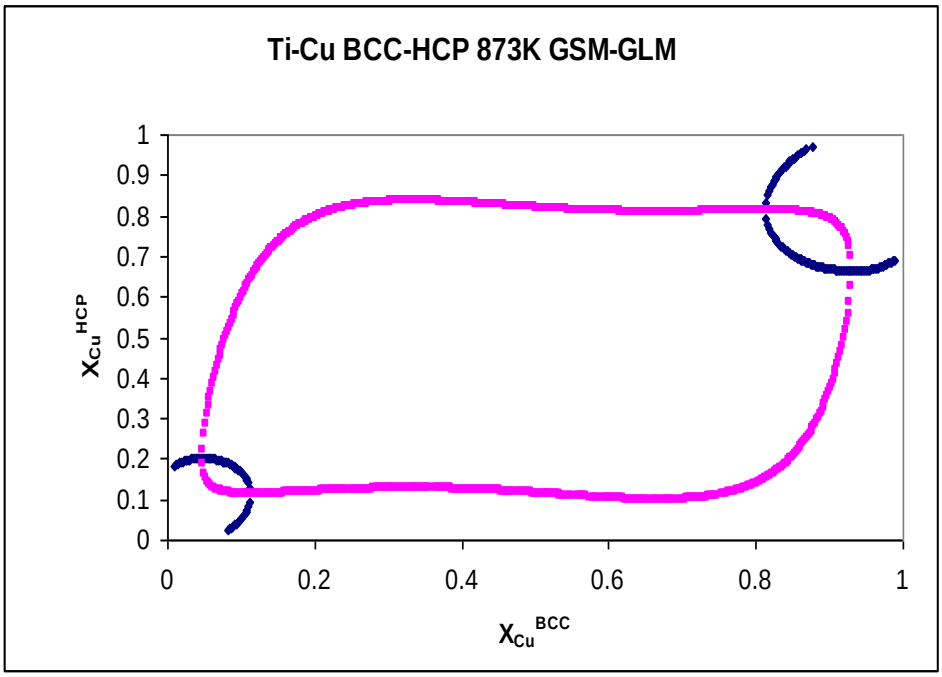

Fig. A.2 Transformation Diagram, Ti-Cu, BCC-HCP, 873 K

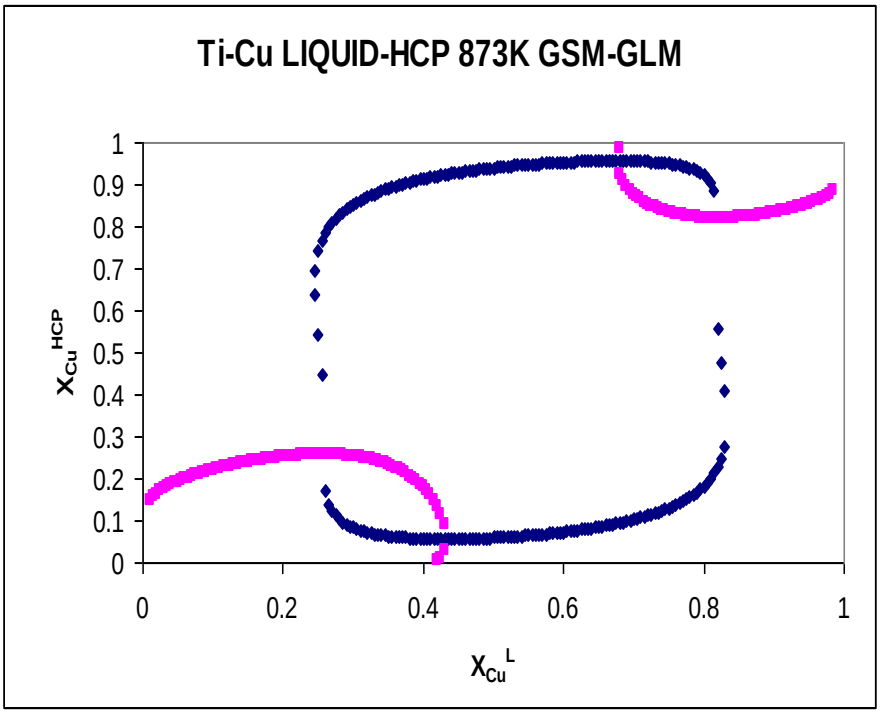

Fig. A.3 Transformation Diagram, Ti-Cu, Liquid-HCP, 873 K